Article

Generation of 3D lacrimal gland organoids from human pluripotent stem cells

https://doi.org/10.1038/s41586-022-04613-4

Received: 4 September 2020

Accepted: 28 February 2022

Published online: 20 April 2022

Check for updates

Ryuhei Hayashi[1,2,3,8]✉, Toru Okubo[1,4,8], Yuji Kudo[1,4], Yuki Ishikawa[1,2], Tsutomu Imaizumi[1,4], Kenji Suzuki[1,2], Shun Shibata[1,4,5], Tomohiko Katayama[2], Sung-Joon Park[6], Robert D. Young[7], Andrew J. Quantock[7] & Kohji Nishida[2,3]

Lacrimal glands are the main exocrine glands of the eyes. Situated within the orbit, behind the upper eyelid and towards the temporal side of each eye, they secrete lacrimal fluid as a major component of the tear film. Here we identify cells with characteristics of lacrimal gland primordia that emerge in two-dimensional eye-like organoids cultured from human pluripotent stem cells[1]. When isolated by cell sorting and grown under defined conditions, the cells form a three-dimensional lacrimal-gland-like tissue organoid with ducts and acini, enabled by budding and branching. Clonal colony analyses indicate that the organoids originate from multipotent ocular surface epithelial stem cells. The organoids exhibit notable similarities to native lacrimal glands on the basis of their morphology, immunolabelling characteristics and gene expression patterns, and undergo functional maturation when transplanted adjacent to the eyes of recipient rats, developing lumina and producing tear-film proteins.

Lacrimal glands act in concert with lipid-producing meibomian glands, which are located inside the eyelids, to jointly establish and maintain a healthy tear film that facilitates good vision. The lacrimal glands also protect the ocular surface by synthesizing defence proteins, including lactoferrin and lysozyme[2]. Lacrimal gland dysfunction and the decreased production of tears is associated with a range of aetiologies, and is a feature of one of the most common autoimmune diseases, Sjögren's syndrome, in which it causes dry-eye syndrome[3,4]. Fetal mammalian lacrimal gland cells have regenerative capabilities[5], and the existence of tissue stem/progenitor cells has been reported previously[6–10]. However, in adult humans, the regenerative ability of the lacrimal gland seems to be minimal, although detailed information is limited by difficulties both in the isolation of cells and the availability of biopsies of gland tissue for research. This identifies the lacrimal gland as a target for research aimed at regenerative therapy and drug discovery using human pluripotent stem (PS) cells, whether derived from embryonic stem (ES) cells or induced PS (iPS) cells. We previously reported the generation of a two-dimensional (2D) eye-like organoid called a self-formed, ectodermal, autonomous, multi-zone (SEAM) organoid from human iPS (hiPS) cells that partially recapture the mechanisms underlying ocular development[1,11]. SEAMs contain precursor cells of a range of ocular tissue lineages, and we showed how corneal and conjunctival epithelial-like cells could be isolated from SEAMs and formed into functional epithelial tissues[12,13]. Here we describe the generation of three-dimensional (3D) lacrimal-gland-like tissue organoids from human ES cells and hiPS cells.

Lacrimal-gland-like primordia in SEAMs

SEAMs were generated from the 201B7 hiPS cell line according to published protocols[1,11] (Extended Data Fig. 1a). After 8 weeks of differentiation, these organoids contained retinal-like cells in SEAM zone 2, α-crystallin-expressing lens-like cells at the margin of zones 2 and 3, and ocular surface epithelial-like cells, co-expressing PAX6 and p63, in zone 3 (Fig. 1a). No endodermal or mesodermal genes were expressed (Extended Data Fig. 1b), confirming that a SEAM recaptures ectoderm-derived ocular development[11] (Fig. 1b). At 10 weeks of differentiation, clusters of cells emerged in SEAM zone 3 that expressed the ocular cell marker PAX6 (ref. [14]), and gland cell markers CD44 (ref. [15]) (Fig. 1c, d), SOX9 (ref. [16]) (Fig. 1e, f) and AQP5 (Extended Data Fig. 1c, d). Some of the $CD44^+$ cells showed evidence of budding and weakly expressed the gland cell marker HTN1 (ref. [17]) (Extended Data Fig. 1e). Accordingly, we conjectured that the induced clusters might represent primordial lacrimal-gland-like cells. To investigate this, the clusters were manually isolated from SEAM zone 3 and cultured in 3D in Matrigel and a medium containing epidermal growth factor (EGF), keratinocyte growth factor (KGF), fibroblast growth factor 10 (FGF10), bone morphogenetic protein 7 (BMP7) and Y-27632, all of which are considered to be key factors required for gland development[18–21]. The clusters began budding at around day 4, had developed multiple branches by day 15 and, by day 39, had formed a 3D structure reminiscent of a lacrimal-gland-like tissue organoid (Fig. 1g). This indicates that SEAM zone 3, which has been shown to contain ocular surface epithelial-like cells[11–14], also engenders precursors of the lacrimal gland.

[1]Department of Stem Cells and Applied Medicine, Osaka University Graduate School of Medicine, Osaka, Japan. [2]Department of Ophthalmology, Osaka University Graduate School of Medicine, Osaka, Japan. [3]Institute for Open and Transdisciplinary Research Initiatives, Osaka University, Osaka, Japan. [4]Basic Research Development Division, ROHTO Pharmaceutical, Osaka, Japan. [5]Department of Informative Genetics, Tohoku University Graduate School of Medicine, Sendai, Japan. [6]Laboratory of Functional Analysis In Silico, Human Genome Center, Institute of Medical Science, University of Tokyo, Tokyo, Japan. [7]School of Optometry and Vision Sciences, Cardiff University, Cardiff, UK. [8]These authors contributed equally: Ryuhei Hayashi, Toru Okubo. ✉e-mail: ryuhei.hayashi@ophthal.med.osaka-u.ac.jp

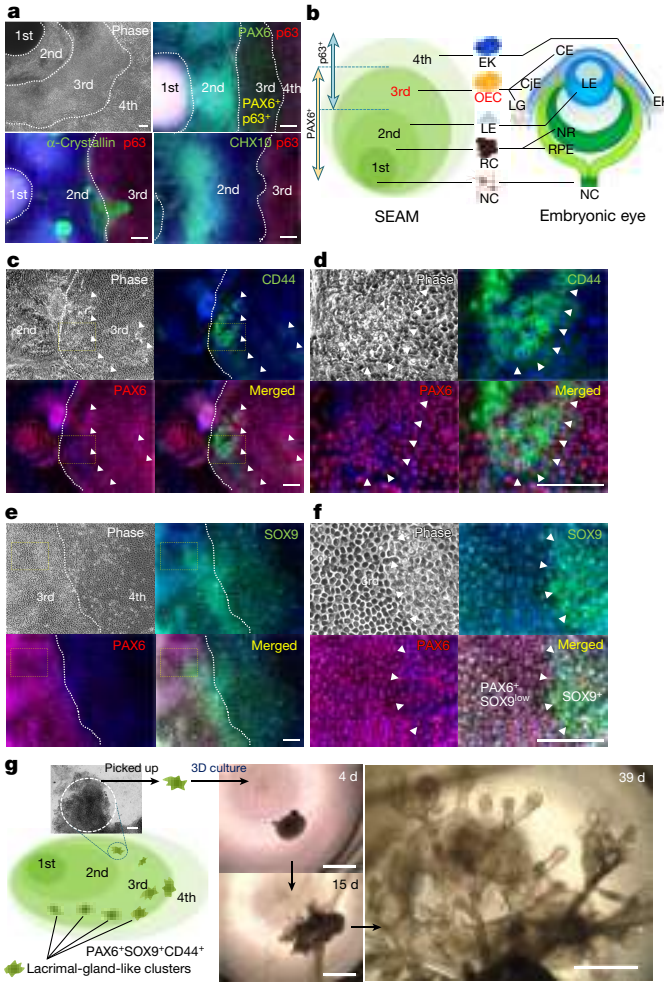

Fig. 1 | Development of lacrimal-gland-like clusters in a SEAM. **a**, Immunostaining analysis of PAX6, α-crystallin, CHX10 and p63 in a typical SEAM derived from iPS cells. $n = 3$ biological replicates. The four zones within the SEAM are indicated as the 1st, 2nd, 3rd and 4th from the centre outwards. Nuclei are shown in blue. Scale bars, 100 µm. **b**, Schematic of a SEAM organoid, with four zones indicated, corresponding to an embryonic eye. CE, corneal epithelial cell; CjE, conjunctival epithelial cell; EK, epidermal keratinocyte; LE, lens; LG, lacrimal gland; OEC, ocular surface epithelial cell; NC, neuronal cell; NR, neuroretina; RC, retinal cell; RPE, retinal pigment epithelium. **c**, **d**, Immunostaining analysis of CD44 and PAX6 in a 10 week SEAM (**c**) with magnified views of the area indicated by dashed boxes (**d**). $n = 3$ biological replicates. The arrowheads indicate cell clusters. Nuclei are shown in blue. For **c** and **d**, scale bars, 100 µm. **e**, **f**, Immunostaining analysis of SOX9 and PAX6 in a 10 week SEAM (**e**) with magnified views of the area indicated by dashed boxes (**f**). $n = 3$ biological replicates. The arrowheads indicate cell clusters. Nuclei are shown in blue. For **e** and **f**, scale bars, 100 µm. **g**, 3D culture of an isolated lacrimal-gland-like cluster at days 4, 15 and 38. $n = 25$ clusters from three independent experiments. Scale bars, 200 µm (left) and 1,000 µm (middle and right).

Sorting of lacrimal-gland-like primordia

Cells obtained from isolated lacrimal-gland-like clusters were analysed using flow cytometry using a previously determined combination of antibodies (anti-ITGB4, anti-SSEA-4 and anti-CD200) that identifies ocular surface epithelial stem cells[12,22]. Approximately 90% of the cells tested were negative for CD200 as a marker of undifferentiated PS cells and neuroectoderm, whereas 60% were ITGB4$^+$SSEA-4$^+$ (Extended Data Fig. 1f). Together, these are characteristics of ocular surface epithelial stem cells. It was therefore concluded that lacrimal-gland-like cell clusters are incorporated within ocular surface epithelial stem cell populations within a SEAM. An analysis of whole SEAMs revealed that the majority of cells were CD200$^+$ (approximately 70%), and that around 40% of the remaining CD200$^-$ cells were ITGB4$^+$SSEA-4$^+$ (Fig. 2a). To examine the ability of the cells to form lacrimal-gland-like structures, each of four CD200$^-$ populations (that is, P1, ITGB4$^-$SSEA-4$^-$; P2, ITGB4$^+$SSEA-4$^-$; P3, ITGB4$^+$SSEA-4$^+$; P4, ITGB4$^-$SSEA-4$^+$) was sorted and processed for 3D culture after spheroid formation for 1 day. By day 3, only the P3 fraction showed budding, with a multibranched gland-like morphology emerging at day 14 (Fig. 2b, Extended Data Fig. 1g and Supplementary Video 1). Accordingly, this cell population (that is, CD200$^-$ITGB4$^+$SSEA-4$^+$) was identified as the origin of lacrimal-gland-like organoids fabricated from hiPS cells.

Lacrimal-gland-like organoid formation

Spheres prepared from the P3 ocular surface epithelial stem cell fraction were cultured in a variety of different media to ascertain the optimal medium for lacrimal-gland-like organoid formation. This revealed that budding and branching were promoted only when the culture medium contained either (1) EGF, Y-27632, KGF, FGF10 and BMP7; or (2) EGF and Y-27632 (EGF/Y-27632 medium) (Fig. 2c and Extended Data Fig. 1h). The induced morphology and gene expression patterns of emerging organoids cultured in these two media were broadly similar, with differentiation markers such as CD44 and AQP5 upregulated after cultivation in EGF/Y-27632 medium (Extended Data Fig. 1i). Thus, the EGF/Y-27632 medium was selected for the ongoing experiments (Supplementary Discussion 1). Lacrimal-gland-like tissue organoids were formed from 201B7 and YZWJs524 hiPS cells and from KhES-1 human ES cells; therefore, their generation seems to apply to human PS cells in general (Extended Data Fig. 2a–e and Supplementary Discussion 2).

Light-sheet fluorescence microscopy analysis of whole-mount 201B7-derived lacrimal-gland-like tissue organoids immunostained with lacrimal gland-related markers identified SOX9 in the nucleus of some acinar cells along with AQP5 (refs. [23,24]) chiefly on acinar cells, where it exhibited a punctate staining pattern (Fig. 2d, e and Supplementary Video 2). We also observed CDH1 (ref. [5]) intracellularly, PAX6 in the nucleus and KRT14 (ref. [25]) in the cytoplasmic region of the majority of cells, with CD44 identified on the entire basal side of all acinar and ductal cells (Extended Data Fig. 3a–c). Similarly, examination of thin sections detected widespread immunostaining of KRT14, punctate staining of AQP5, with CD44 immunoreactivity seen in the outer layers of the acini (Fig. 2f). No clear lumen structures were observed in morphological sections (Extended Data Fig. 3d), but intracellular CDH1 and intranuclear PAX6 were present in the hiPS-cell-derived lacrimal-gland-like organoids (Extended Data Fig. 3e), and AQP5 and SOX9 were identified in some acinar cells (Extended Data Fig. 3f). However, the signal for the myoepithelial marker ACTA2 (refs. [26,27]) was low to negligible (Extended Data Fig. 3f). Organoids generated from human ES cells showed similar immunostaining patterns to their hiPS-cell-derived counterparts (Extended Data Fig. 3g–i).

Gene expression analyses revealed that transcription factors involved in lacrimal gland development such as *PAX6*, *SOX9*, *BARX2* (ref. [28]), *RUNX1* (ref. [29]), *SIX2* (ref. [30]) and *FGFR2IIIb* were transiently upregulated during lacrimal gland differentiation culture, and subsequently decreased in the lacrimal-gland-like organoids (Fig. 2g and Extended Data Fig. 3j). Single-cell RNA-seq (scRNA-seq) analysis indicated that, at day 10 of 3D cultivation, lacrimal-gland-like progenitors transiently expressed the proliferation marker *MKI67* along with epithelial-mesenchymal transition markers *VIM* and *FN1*. Expression of these markers decreased by day 20, by which time AQP5$^+$ acinar cells had started to express the functional lacrimal gland proteins *LCN2* (ref. [8]) and *DEFB1* (ref. [31]), for lipocalin and defensin, respectively (Extended Data Fig. 4a–c and Supplementary Table 1). Moreover, the day-20 organoids contained major cell clusters including acinar,

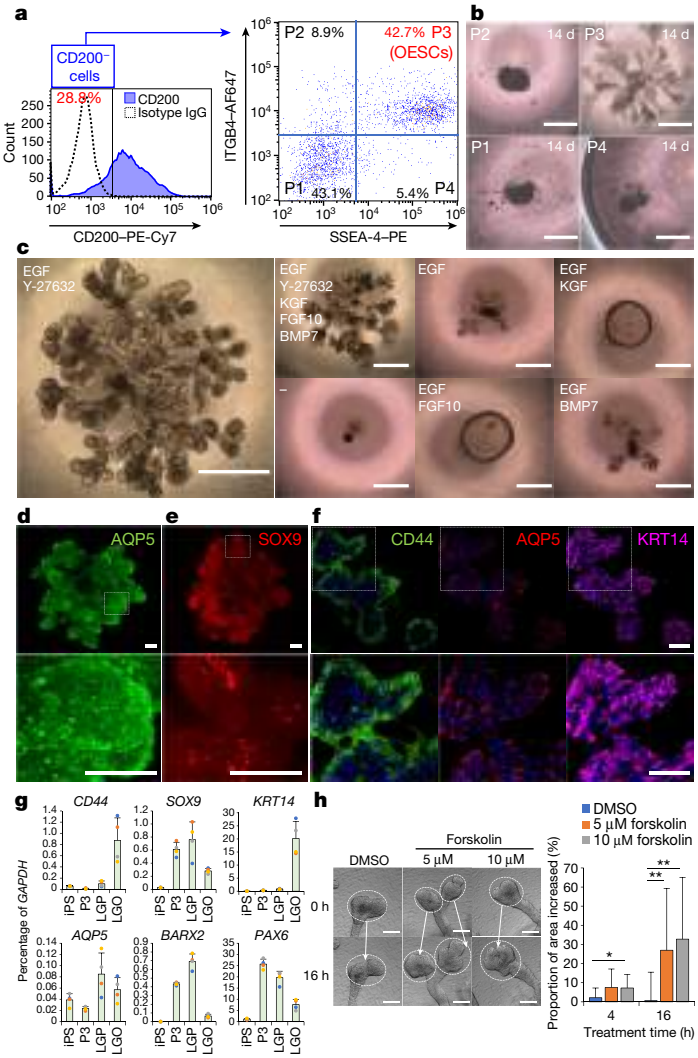

Fig. 2 | Generation and characterization of lacrimal-gland-like organoids. **a**, Flow cytometry analysis of SSEA-4, ITGB4 and CD200 in SEAMs. $n = 91$ cell sortings. OESCs, ocular surface epithelial stem cells. **b**, 3D culture of the sorted cell populations. $n = 5$ biological replicates. Scale bars, 1,000 μm. **c**, Screening for organoid induction medium. $n = 3$ biological replicates. Scale bars, 1,000 μm. **d**, **e**, Light-sheet fluorescence microscopy analysis of lacrimal-gland-like organoids stained with anti-AQP5 (**d**) and anti-SOX9 (**e**) antibodies. The bottom panels show magnified views of the top panels. $n = 2$ biological replicates. Scale bars, 200 μm. **f**, Immunostaining analysis of CD44, AQP5 and KRT14 in thin sections of lacrimal-gland-like organoids. The bottom panels show magnified views of the top panels. $n = 3$ biological replicates. Nuclei are shown in blue. Scale bars, 100 μm. **g**, Gene expression analysis of lacrimal gland markers in iPS cells, P3 cells, lacrimal-gland-like progenitors (LGP) and organoids (LGO). $n = 4$ biological replicates. Data are mean ± s.d. **h**, Swelling assay using forskolin for lacrimal-gland-like organoids. Scale bars, 200 μm. $^{*}P < 0.05$, $^{**}P < 0.01$. Distinct endbuds from three independent experiments were examined: $n = 25$ (DMSO) and $n = 23$ (forskolin). Data are mean ± s.d. Exact *P* values are provided in the source data.

ductal and myoepithelial-like cells (Extended Data Fig. 4d, Supplementary Table 2 and Supplementary Discussion 3). Swelling assays to evaluate water/ion transport abilities revealed that the end buds of lacrimal-gland-like organoids responded to treatment with forskolin in a time-dependent manner (Fig. 2h). This swelling ability is characteristic of exocrine gland function, and the fact that it was observed at levels lower compared with those reported for adult lacrimal gland cells[9] was not unexpected, given that the hiPS-cell-derived organoids as proxies of lacrimal glands are not fully mature in vitro (Supplementary Discussion 4).

Origin of lacrimal-gland-like progenitors

To investigate the hypothesis that lacrimal-gland-like progenitors are derived from ocular surface epithelial stem cells, we used time-lapse microscopy to observe clonal colony formation, classified as either domed or flat (Fig. 3a). Almost all of the colonies were initially dome shaped, but over time tended to morph into flat colonies to such an extent that, after 4 weeks, flat colonies were predominant (Fig. 3b). Domed colonies are more effective than flat colonies in inducing lacrimal-gland-like tissue organoids (Fig. 3c, d); prolonged cultivation in 2D of ocular surface epithelial stem cells leads to cellular stratification and the emergence of a corneal epithelial phenotype (Extended Data Fig. 5a–c). Genes associated with lacrimal gland development, such as *BARX2*, *SIX2* (ref. [30]), *SOX9* and *KRT15* (ref. [23]), were upregulated in domed colonies (Extended Data Fig. 5d, e). By contrast, in flat colonies, mucosal epithelial keratin, *KRT13*, and the corneal epithelial progenitor cell markers, *CDH2* and *NGFR*, predominated[32,33]. *YAP1* was also upregulated as well as its downstream genes *CTGF* and *CYR61* (ref. [34]), which are involved in corneal epithelial development[22]. YAP1 protein was identified in the nuclei of cells in flat colonies and in the cytoplasm of cells in domed colonies (Extended Data Fig. 5f). This indicates that YAP signalling negatively regulates the development of lacrimal-gland-like organoids (Supplementary Discussion 5).

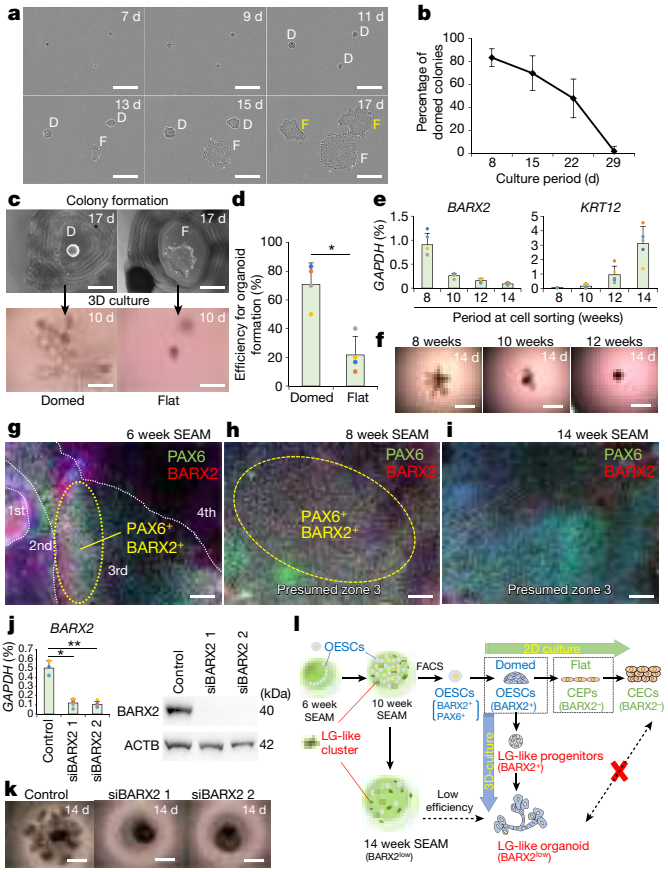

Fig. 3 | Characterization of lacrimal-gland-like primordia. a, Time-lapse images of colony formation using P3 ocular surface epithelial stem cells. Domed (D) and flat (F) colonies are indicated. Scale bars, 400 µm. **b**, The proportion of domed colonies during colony formation. $n = 6$ biological replicates. Data are mean ± s.d. **c**, **d**, Generation of lacrimal-gland-like organoids from domed and flat colonies (**c**) and their efficiency to form lacrimal-gland-like organoids (**d**). Scale bars, 1,000 µm (**c**, top), 400 µm (**c**, bottom). $^*P < 0.05$. $n = 4$ biological replicates. Data are mean ± s.d. Exact *P* values are provided in the source data. **e**, The expression of *BARX2* and *KRT12* in P3 ocular surface epithelial stem cells sorted at different culture periods. $n = 5$ biological replicates. Data are mean ± s.d. **f**, Organoid formation using P3 ocular surface epithelial stem cells sorted at different culture periods. $n = 4$ biological replicates. Scale bars, 1,000 µm. **g**–**i**, Immunostaining analysis of PAX6 and BARX2 in 6 week (**g**), 8 week (**h**) and 14 week (**i**) SEAMs. $n = 2$ biological replicates. Nuclei are shown in blue. For **g**–**i**, scale bars, 100 µm. **j**, **k**, Gene knockdown of *BARX2* using siRNA (**j**) and the effect on organoid formation (**k**). $^*P < 0.05$, $^{**}P < 0.01$. $n = 5$ biological replicates. Data are mean ± s.d. Exact *P* values are provided in the source data. For **k**, scale bars, 1,000 µm. **l**, Schematic of ocular surface epithelial stem cells (OESCs) and lacrimal-gland-like organoid development. CECs, corneal epithelial cells; CEPs, corneal epithelial progenitors.

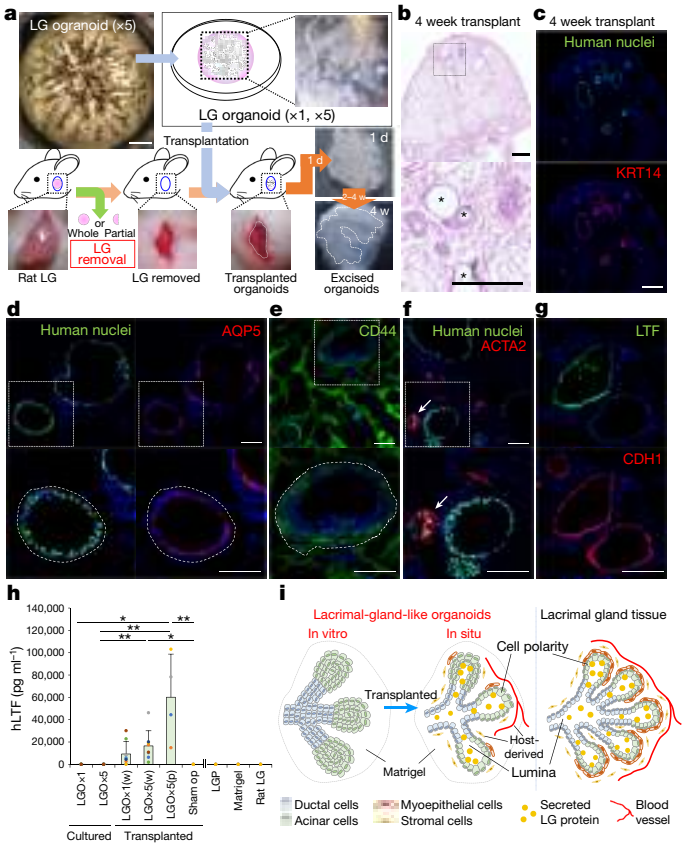

Fig. 4 | Transplantation of lacrimal-gland-like organoids. a, Schematic of the transplantation of lacrimal-gland-like organoids into immunodeficient rats. Scale bar, 1,000 µm. **b**, Haematoxylin and eosin (H&E) staining of 4 week transplanted tissue. Magnified views of the top images are shown at the bottom. Scale bars, 500 µm. The asterisks indicate lumina. **c**–**g**, Transplanted organoids (×5) four weeks after implantation, immunostained for human nuclei along with KRT14 (**c**), AQP5 (**d**), CD44 (**e**), ACTA2 (**f**), and LTF and CDH1 (**g**). The bottom panels in **d**–**f** show magnified views of the top panels. The dotted lines in **d** and **e** indicate the basal side of the organoids. The arrows in **f** indicate human myoepithelial-like cells. For **c**–**g**, scale bars, 100 µm. $n = 3$ biological replicates (**b**–**g**). **h**, ELISA analysis of human lactoferrin (hLTF) in lacrimal-gland-like organoids (LGOs). Whole (w) and partial (p) lacrimal gland-removal surgeries are indicated. $^*P < 0.05$, $^{**}P < 0.01$. $n = 8$ (LGO×1, LGO×5, LGO×1(w) and LGO×5(w)) and $n = 4$ (others) biological replicates). Data are mean ± s.d. Exact *P* values are provided in the source data. **i**, Schematic of SEAM-derived lacrimal-gland-like organoids and lacrimal gland tissue.

Immunostaining analysis of domed colonies showed high expression of BARX2 protein, an important transcriptional factor for lacrimal gland development[28,30] (Extended Data Fig. 6a). *BARX2* gene expression during SEAM differentiation indicated that mRNA levels were higher in the early stages of SEAM formation (that is, at 8 weeks) than at later time-points (that is, at 12–14 weeks). By contrast, *KRT12*, a marker of corneal differentiation, increased as the culture period lengthened (Fig. 3e). The propensity for SEAM-derived ocular surface epithelial stem cells to engender lacrimal-gland-like organoid formation diminished over time (Fig. 3f), with prolonged culture periods reducing both total colony formation and the relative proportion of domed colonies progressing to develop lacrimal-gland-like organoids (Extended Data Fig. 6b).

BARX2 was co-expressed with PAX6 in the innermost region of SEAM zone 3 at 6 and 8 weeks of differentiation. Thereafter, BARX2 expression reduced, in contrast to KRT12 expression, which increased with time (Fig. 3g–i and Extended Data Fig. 6c, d). Moreover, BARX2 was strongly expressed in spheroids formed by lacrimal-gland-like progenitors, but was decreased in lacrimal-gland-like organoids (Extended Data Fig. 6e). *BARX2* knockdown using short interfering RNA (siRNA) caused a significant reduction of budding and branching in the 3D culture of lacrimal-gland-like spheroids (Fig. 3j, k and Supplementary Fig. 1) and in the formation of domed colonies in 2D culture, but with no significant effect on corneal epithelial differentiation (Extended Data Fig. 6f, g). This confirms that BARX2 is a key molecule in lacrimal gland development and is influential in the formation of lacrimal-gland-like tissue organoids generated from hiPS cells.

hiPS-cell-derived corneal epithelium induced in 2D culture is unable to transform into lacrimal-gland-like tissue organoids (Extended Data Fig. 7a). Similarly, lacrimal-gland-like organoids fabricated in 3D culture cannot form a corneal epithelium (Extended Data Fig. 7b–f). Moreover,

lacrimal-gland-like organoids cannot be maintained by long-term cultivation or by cell passaging (Extended Data Fig. 7g, h). Thus, although lacrimal-gland-like and corneal epithelial-like progenitor cells derived from SEAM zone 3 share a similar origin as multipotent ocular surface epithelial stem cells, they are unable to secondarily transdifferentiate after the initial differentiation into a specific lineage (Fig. 3l).

Transplantation studies

Lacrimal-gland-like organoids, generated from either one or five lacrimal-gland-like precursor spheroids, were transplanted into the connective tissue near the eyes of rats from which the lacrimal gland had been partially or completely removed (Fig. 4a and Extended Data Fig. 8a, b). One day after transplantation, implanted human lacrimal-gland-like organoid material was identified in the rat lacrimal gland tissue. Four weeks after surgery, engrafted human lacrimal gland cells persisted, some of which exhibited lumen-like structures (Fig. 4b, c). The majority of these human cells expressed KRT14, PAX6 and CDH1, while a proportion expressed AQP5 apically, with SOX9 present in the nuclei and CD44 (not merged with CD31) seen basally, indicating the emergence of cell polarity (Fig. 4d, e and Extended Data Fig. 8c–e). In contrast to the in vitro lacrimal-gland-like tissue organoids, those that had been transplanted showed clear ductal tube formation 2 weeks after implantation, which became more pronounced at the 4 week time point (Extended Data Fig. 8f–k). Although most of the $ACTA2^+$ cells that accumulated around the transplanted lacrimal-gland-like organoids were rat stromal cells (that is, non-human, $CD31^-$ cells), in some sections, a few cells reacted positively with anti-human antibodies, suggesting that lacrimal-gland-like organoids might be able to differentiate into $ACTA2^+$ human myoepithelial-like cells (Fig. 4f and Extended Data Fig. 8l). Lactoferrin-expressing secretory gland cells, which could not be seen in lacrimal-gland-like organoids in vitro, were also detected in some parts of the transplanted organoids (Fig. 4g). Transmission electron microscopy analysis of the lacrimal-gland-like organoids 4 weeks after implantation (Extended Data Fig. 9a–h) detected many of the defining features of human lacrimal gland[35] (Supplementary Discussion 6).

Enzyme-linked immunosorbent assays (ELISAs) indicated that the levels of human lactoferrin and lysozyme proteins were elevated in transplanted lacrimal-gland-like tissue organoids compared with non-transplanted organoids or tissue from sham operations. Protein levels were also higher in transplanted lacrimal-gland-like organoids that had been generated from five lacrimal-gland-like spheroids compared with those derived from single spheres. Levels were also higher in the case of a partial, rather than total, gland removal surgery (Fig. 4h and Extended Data Fig. 9i), indicating that both the microenvironment of the transplanted site and the number of transplanted organoids are important for lacrimal-gland-like organoids to achieve functional maturity. It is also probable that, in the partial removal model, migrating host lacrimal gland cells (especially mesenchymal stromal cells) and host lacrimal-gland-derived cytokines promote the maturation and survival of transplanted lacrimal-gland-like organoids.

Lactoferrin production in transplanted organoids (Fig. 4h) reached approximately half of that achieved in rat lacrimal tissue in vivo (Extended Data Fig. 9j). Gene expression analysis of the tissues after transplantation using human gene-specific TaqMan probe sets (Supplementary Table 3) revealed a 3,000 times higher expression of *LYZ* and *LTF*, encoding the tear-film proteins lysozyme and lactoferrin, in transplanted lacrimal-gland-like tissue organoids compared with non-transplanted ones, in addition to an increased expression of the lacrimal gland-related differentiation markers *CD44* and *AQP5* (Extended Data Fig. 9k). The expression phenotypes of the transplanted lacrimal-gland-like organoids are therefore consistent with those of lacrimal gland tissue, but not other glandular or ocular surface epithelial tissues (Extended Data Fig. 10a–d).

In conclusion, we describe the generation of lacrimal-gland-like tissue organoids from hiPS cells and ES cells. The data suggest that lacrimal gland maturation starts during in vitro 3D culture and continues in situ after implantation (Fig. 4i). This advance holds promise for future studies of lacrimal gland development and for use in future regenerative therapies to treat disorders such as Sjögren's syndrome, once appropriate surgical transplant procedures have been developed. The organoids also have tangible benefits for application in the fields of drug development for treatment of lacrimal gland-related disease[36–39], and as a platform for investigations of glandular pathology through the generation of disease-specific hiPS cells.

Online content

Any methods, additional references, Nature Research reporting summaries, source data, extended data, supplementary information, acknowledgements, peer review information; details of author contributions and competing interests; and statements of data and code availability are available at https://doi.org/10.1038/s41586-022-04613-4.

1. Hayashi, R. et al. Co-ordinated ocular development from human iPS cells and recovery of corneal function. *Nature* **531**, 376–380 (2016).
2. Janssen, P. & Van Bijsterveld, O. Origin and biosynthesis of human tear fluid proteins. *Invest. Ophthalmol. Vis. Sci.* **24**, 623–630 (1983).
3. Ramos-Casals, M., Tzioufas, A. G., Stone, J. H., Sisó, A. & Bosch, X. Treatment of primary Sjögren syndrome: a systematic review. *JAMA* **304**, 452–460 (2010).
4. Pflugfelder, S. C., Solomon, A. & Stern, M. E. The diagnosis and management of dry eye: a twenty-five–year review. *Cornea* **19**, 644–649 (2000).
5. Hirayama, M. et al. Functional lacrimal gland regeneration by transplantation of a bioengineered organ germ. *Nat. Commun.* **4**, 2497 (2013).
6. Shatos, M. A., Haugaard-Kedstrom, L., Hodges, R. R. & Dartt, D. A. Isolation and characterization of progenitor cells in uninjured, adult rat lacrimal gland. *Invest. Ophthalmol. Vis. Sci.* **53**, 2749–2759 (2012).
7. Kobayashi, S. et al. Characterization of cultivated murine lacrimal gland epithelial cells. *Mol. Vis.* **18**, 1271–1277 (2012).
8. Bannier-Hélaouët, M. et al. Exploring the human lacrimal gland using organoids and single-cell sequencing. *Cell Stem Cell* **28**, 1221–1232 (2021).
9. Basova, L. et al. Origin and lineage plasticity of endogenous lacrimal gland epithelial stem/progenitor cells. *iScience* **23**, 101230 (2020).
10. Jeong, S. Y. et al. Establishment of functional epithelial organoids from human lacrimal glands. *Stem Cell Res. Ther.* **12**, 247 (2021).
11. Hayashi, R. et al. Coordinated generation of multiple ocular-like cell lineages and fabrication of functional corneal epithelial cell sheets from human iPS cells. *Nat. Protoc.* **12**, 683–696 (2017).
12. Hayashi, R., Ishikawa, Y., Katayama, T., Quantock, A. J. & Nishida, K. CD200 facilitates the isolation of corneal epithelial cells derived from human pluripotent stem cells. *Sci. Rep.* **8**, 16550 (2018).
13. Nomi, K. et al. Generation of functional conjunctival epithelium, including goblet cells, from human iPSCs. *Cell Rep.* **34**, 108715 (2021).
14. Makarenkova, H. P. et al. FGF10 is an inducer and Pax6 a competence factor for lacrimal gland development. *Development* **127**, 2563–2572 (2000).
15. Yoshida, K., Nitatori, T. & Uchiyama, Y. Localization of glycosaminoglycans and CD44 in the human lacrimal gland. *Arch. Histol. Cytol.* **59**, 505–513 (1996).
16. Chen, Z. et al. FGF signaling activates a Sox9-Sox10 pathway for the formation and branching morphogenesis of mouse ocular glands. *Development* **141**, 2691–2701 (2014).
17. Shah, D. et al. Histatin-1 expression in human lacrimal epithelium. *PLoS ONE* **11**, e0148018 (2016).
18. Ohuchi, H. et al. FGF10 acts as a major ligand for FGF receptor 2 IIIb in mouse multi-organ development. *Biochem. Biophys. Res. Commun.* **277**, 643–649 (2000).
19. Dean, C., Ito, M., Makarenkova, H. P., Faber, S. C. & Lang, R. A. Bmp7 regulates branching morphogenesis of the lacrimal gland by promoting mesenchymal proliferation and condensation. *Development* **131**, 4155–4165 (2004).
20. Lin, H., Liu, Y. & Yiu, S. Three dimensional culture of potential epithelial progenitor cells in human lacrimal gland. *Transl. Vis. Sci. Technol.* **8**, 32 (2019).
21. Farmer, D. T. et al. miR-205 is a critical regulator of lacrimal gland development. *Dev. Biol.* **427**, 12–20 (2017).
22. Shibata, S. et al. Selective laminin-directed differentiation of human induced pluripotent stem cells into distinct ocular lineages. *Cell Rep.* **25**, 1668–1679 (2018).
23. Ishida, N., Hirai, S.-I. & Mita, S. Immunolocalization of aquaporin homologs in mouse lacrimal glands. *Biochem. Biophys. Res. Commun.* **238**, 891–895 (1997).
24. Tsubota, K., Hirai, S., King, L. S., Agre, P. & Ishida, N. Defective cellular trafficking of lacrimal gland aquaporin-5 in Sjögren's syndrome. *Lancet* **357**, 688–689 (2001).
25. Hirayama, M., Liu, Y., Kawakita, T., Shimmura, S. & Tsubota, K. Cytokeratin expression in mouse lacrimal gland germ epithelium. *Exp. Eye Res.* **146**, 54–59 (2016).
26. Farmer, D. T. et al. Defining epithelial cell dynamics and lineage relationships in the developing lacrimal gland. *Development* **144**, 2517–2528 (2017).
27. Makarenkova, H. P. & Dartt, D. A. Myoepithelial cells: their origin and function in lacrimal gland morphogenesis, homeostasis, and repair. *Curr. Mol. Biol. Rep.* **1**, 115–123 (2015).

28. Tsau, C. et al. Barx2 and Fgf10 regulate ocular glands branching morphogenesis by controlling extracellular matrix remodeling. *Development* **138**, 3307–3317 (2011).
29. Voronov, D. et al. *T*ranscription factors Runx1 to 3 are expressed in the lacrimal gland epithelium and are involved in regulation of gland morphogenesis and regeneration. *Invest. Ophthalmol. Vis. Sci.* **54**, 3115–3125 (2013).
30. Hirayama, M. et al. Identification of transcription factors that promote the differentiation of human pluripotent stem cells into lacrimal gland epithelium-like cells. *NPJ Aging Mech. Dis.* **3**, 1 (2017).
31. Haynes, R. J., Tighe, P. J. & Dua, H. S. Antimicrobial defensin peptides of the human ocular surface. *Br. J. Ophthalmol.* **83**, 737–741 (1999).
32. Hayashi, R. et al. N-Cadherin is expressed by putative stem/progenitor cells and melanocytes in the human limbal epithelial stem cell niche. *Stem Cells* **25**, 289–296 (2007).
33. Girolamo, N. D. et al. Localization of the low-affinity nerve growth factor receptor p75 in human limbal epithelial cells. *J. Cell. Mol. Med.* **12**, 2799–2811 (2008).
34. Moroishi, T. et al. A YAP/TAZ-induced feedback mechanism regulates Hippo pathway homeostasis. *Genes Dev.* **29**, 1271–1284 (2015).
35. Bron, A. J., Tripathi, R. C. & Tripathi, B. J. *Wolff's Anatomy of the Eye and Orbit* 8th Edn, 72–75 (Chapman & Hall, 1997).
36. Avila, M. Y. Restoration of human lacrimal function following platelet-rich plasma injection. *Cornea* **33**, 18–21 (2014).
37. Zhang, Y., Deng, C., Qian, J., Zhang, M. & Li, X. Improvement of radiotherapy-induced lacrimal gland injury by induced pluripotent stem cell-derived conditioned medium via MDK and inhibition of the p38/JNK pathway. *Int. J. Mol. Sci.* **15**, 18407–18421 (2014).
38. Beyazyıldız, E. et al. Efficacy of topical mesenchymal stem cell therapy in the treatment of experimental dry eye syndrome model. *Stem Cells Int.* **2014**, 250230 (2014).
39. Weng, J. et al. Mesenchymal stromal cells treatment attenuates dry eye in patients with chronic graft-versus-host disease. *Mol. Ther.* **20**, 2347–2354 (2012).

Methods

All of the experiments were performed in accordance with the relevant institutional and national guidelines and regulations. No statistical methods were used to predetermine sample size. The experiments were not randomized and the investigators were not blinded to allocation during experiments and outcome assessment. A step-by-step protocol describing the fabrication of lacrimal-gland-like organoids is available at the Protocol Exchange[40].

hPS cells

The hiPS cell line 201B7 and human ES cell line (KhES-1) were purchased from RIKEN BioResource Center. The hiPS cell line YZWJs524 was provided by Kyoto University's Center for iPS Cell Research and Application (CiRA). Cells were cultured on laminin-511 E8 fragments (LN511E8; Nippi) in serum-free medium (StemFit; Ajinomoto)[41]. All of the experiments using recombinant DNA were approved by the Recombinant DNA Committee of Osaka University and were performed according to institutional guidelines. The use of human ES cells was approved by the Ministry of Education, Culture, Sports, Science, and Technology of Japan.

SEAM formation

The components of the differentiation culture medium are shown in Supplementary Table 4. The differentiation of ocular cell lineages from hPS cells was performed according to the previously reported SEAM method[11]. In brief, hPS cells were seeded onto LN511E8-coated (0.5 μg cm^{-2}) plates and cultured in StemFit medium for 10 days, after which the medium was changed to serum-free differentiation medium (DM; GMEM, Thermo Fisher Scientific) supplemented with 10% knockout serum replacement (Thermo Fisher Scientific), 1 mM sodium pyruvate (Thermo Fisher Scientific), 0.1 mM non-essential amino acids (Thermo Fisher Scientific), 2 mM L-glutamine (Thermo Fisher Scientific), 100 U ml^{-1} penicillin potassium and 100 μg ml^{-1} streptomycin sulfate (Meiji Seika Pharma), and 55 μM monothioglycerol (Wako). After four weeks, the medium was replaced with epithelial differentiation medium (EDM; DM and CnT-PR without EGF and FGF2, CELLnTEC Advanced Cell Systems) (1:1) containing 20 ng ml^{-1} KGF (Wako) and 10 μM Y-27632 (Wako), 100 U ml^{-1} penicillin potassium and 100 μg ml^{-1} streptomycin sulfate) and cultured for an additional four weeks. Non-epithelial cells were removed from the SEAM by pipetting, which was performed around 7 weeks after the initiation of differentiation. The medium was then replaced with ocular surface epithelial differentiation medium (OSEM; DMEM/F12 (Thermo Fisher Scientific) containing 2% B-27 supplement (Thermo Fisher Scientific), 20 ng ml^{-1} KGF, 10 μM Y-27632, 100 U ml^{-1} penicillin potassium and 100 μg ml^{-1} streptomycin sulfate), after which the plates were incubated for an additional 0 to 6 weeks according to the experimental purpose (the total time in culture was between 8 and 14 weeks). Phase-contrast microscopy was performed using an Axio observer Z1, D1 (Zeiss) and an EVOS FL Auto (Life Technologies).

Flow cytometry and cell sorting

Flow cytometry and cell sorting were performed as previously reported[12]. For lacrimal-gland-like cell culture, after 10 to 12 weeks of differentiation culture using the SEAM method, cells were collected using Accutase (Thermo Fisher Scientific). Dissociated cells were stained with Alexa Fluor 647 (AF647)-conjugated anti-ITGB4 (450-9D, BD Biosciences), PE-conjugated anti-SSEA-4 (MC813-70, BioLegend) and PE-Cy7-conjugated anti-CD200 antibodies (OX-104, BD Biosciences) for 1 h on ice. Isotype antibodies corresponding to each antibody were used in the control experiments. Flow cytometry and cell sorting were performed using the SH800 cell sorter (Sony Biotechnology) and the FACSAriaII cell sorter (BD Biosciences) according to the manufacturer's instructions. Data were analysed using the SH800 software (Sony Biotechnology), BD FACSDiva Software (BD Biosciences) and FlowJo software (TreeStar). Small debris was removed by gating in the FSC/BSC(SSC) axis, and the doublets were gated out using the axes of FSC-A/FSC-W and BSC(SSC)-A/BSC(SSC)-W. A positive region for each antibody staining was defined as a region that contained almost no cells (that is, <1.0%) stained with the corresponding isotype control antibody. Sorted cells were collected in 8 ml of 2% B-27 supplement containing DMEM/F12 medium in a STEMFULL 15 ml tube (Sumitomo Bakelite).

3D culture of lacrimal-gland-like tissue organoids

Sorted ocular surface epithelial stem cells ($CD200^{-}SSEA\text{-}4^{+}ITGB4^{+}$) were cultured in OSEM in the wells of a non-adhesive, round-bottomed 96-well plate (Sumitomo Bakelite) for 1 day at 1×10^5 cells per well. This resulted in the formation of a spheroid of lacrimal-gland-like progenitors. Spheroids were embedded in 50% (v/v) of Matrigel (growth factor reduced, Corning) diluted in lacrimal gland culture medium (LGM; DMEM/F12 containing 2% B-27 supplement, 10 ng ml^{-1} EGF, 10 μM Y-27632, 100 U ml^{-1} penicillin potassium and 100 μg ml^{-1} streptomycin sulfate) for approximately 20 days. For the screening experiment, 20 ng ml^{-1} KGF, 100 ng ml^{-1} FGF10 (Wako) and 100 ng ml^{-1} BMP7 (Wako)) were used as supplements. Lacrimal-gland-like clusters, which had been induced in 10–14 week SEAMs, were manually isolated under a microscope, after which the cluster was directly embedded in Matrigel and cultured for up to 39 days in LGM or LGM supplemented with 20 ng ml^{-1} KGF, 100 ng ml^{-1} FGF10 and 100 ng ml^{-1} BMP7. Microscopy observations of 3D organoid cultures were performed using the EVOS FL Auto system.

Culture for corneal epithelial differentiation

Cells isolated by cell sorting were seeded onto LN511E8-coated dishes at a density of 1×10^5 cells per well in 12-well plates or cell culture inserts, and cultured in OSEM and corneal epithelium maturation medium (that is, keratinocyte culture medium[11] containing 20 ng ml^{-1} KGF and 10 μM Y-27632) for 14–21 days.

Clonal colony analysis

Ocular surface epithelial stem cells, derived from 8 to 14 week SEAMs, were seeded at 100 or 200 cells per well in six-well uncoated plates and cultured in ocular surface epithelial differentiation medium for 29 days. Domed and flat colonies were distinguished on the basis of morphological differences under phase-contrast microscopy. The numbers of domed and flat colonies were counted, and the proportions of domed/flat colonies and the respective colony-formation efficiency were calculated. For time-lapse imaging, an IncuCyte Live-Cell Imaging System (ESSEN BioScience) was used.

Gene knockdown using siRNA

Formed spheres of lacrimal-gland-like progenitors were dissociated using Accutase. siRNAs (Silencer Select pre-designed and validated for *BARX2*1 (s16242), 2 (s16243) and Negative Control No. 1 siRNA; Thermo Fisher Scientific) were then introduced into the dissociated cells, which were cultured in a non-adhesive, round-bottomed 96-well plate for 18–24 h. The reformed spheres were embedded in Matrigel to induce 3D lacrimal-gland-like differentiation. Gene expression was examined after 3 to 6 days of culture.

Western blot analysis

Lacrimal-gland-like tissue organoids were lysed in ice-cold RIPA buffer (Nacalai Tesque). Samples were then electrophoresed with NuPAGE 4 to 12% Bis-Tris gels (Thermo Fisher Scientific), transferred to PVDF membranes (GE Healthcare Technologies), blocked with 5% skimmed milk in Tris-buffered saline with Tween-20 (TaKaRa Bio) after which membranes were incubated with anti-BARX2 and anti-ACTB antibodies (Supplementary Table 5) at 4 °C overnight. Blots were detected using ECL Select Western Blotting Detection Reagent (GE Healthcare) after

reaction with a HRP-conjugated secondary antibodies (1:5,000; GE Healthcare). The blots were visualized using the Molecular Imager ChemiDoc XRS+ system (Bio-Rad Laboratories, Hercules).

Swelling assay

Swelling assays were performed according to previous reports[42,43]. Lacrimal-gland-like organoids were incubated with 5 or 10 μM forskolin (Tokyo Chemical Industry) for up to 34 h. Morphological changes were photographed hourly using the Axio observer Z1 microscope. The swelling ratios of the gland endbuds within each organoid were analysed by calculating the areas at 0, 4 and 16 h after forskolin addition using ImageJ software v.153e (National Institutes of Health).

Immunofluorescence staining

Sections of gland tissues including human salivary gland, mammary gland and pancreas were obtained from the BioChain Institute. Cells or tissues were fixed in 2–4% paraformaldehyde (Wako), washed with Tris-buffered saline (TaKaRa Bio) three times for 10 min, and incubated with Tris-buffered saline containing 5% normal donkey serum and 0.3% Triton X-100 for 1 h to block non-specific reactions. Afterwards, they were incubated with the antibodies listed in Supplementary Table 5 at 4 °C overnight or at room temperature for 3 h. The cells were again washed three times with Tris-buffered saline for 10 min and incubated with AF488-, AF568- and AF647-conjugated secondary antibodies (1:200; Thermo Fisher Scientific) for 1 h at 22–28 °C. Counterstaining was performed with Hoechst 33342 (Thermo Fisher Scientific) before fluorescence microscopy (Axio Observer D1, Zeiss). Research-grade human corneo-scleral tissue was obtained from CorneaGen.

Light-sheet fluorescence microscopy

Lacrimal-gland-like organoids were fixed in 4% paraformaldehyde, washed with Tris-buffered saline three times for 10 min and incubated in Tris-buffered saline containing 1% donkey serum and 0.3% Triton X-100 for 24 h for blocking and permeabilization. The tissues were then incubated with primary antibodies (Supplementary Table 5) for 24 to 72 h at 4 °C. The tissues were again washed three times with Tris-buffered saline for 10 min and incubated with the corresponding AF488- and AF568-conjugated secondary antibodies (Thermo Fisher Scientific) for 1 h at room temperature. Counterstaining was performed with Hoechst 33342 (Molecular Probes, Eugene). The samples were observed with a fluorescence microscope (Lightsheet Z.1, Zeiss) according to the manufacturer's instructions. For analyses of 3D microscopy images, Imaris v.6 (Zeiss) was used.

H&E staining

Tissue slides of lacrimal-gland-like organoids were fixed with 10% formaldehyde neutral buffer solution (Nacalai Tesque). The sections were stained with H&E, after which the sections were imaged using a BZ-9000 microscope (Keyence).

Transmission electron microscopy analysis

Organoids or transplanted tissues were immersed in 2.5% glutaraldehyde/2% paraformaldehyde (Nacalai Tesque) in 0.1 M sodium phosphate buffer pH 7.2 and incubated on a rotator for 3 h at room temperature. The fixed samples were then transferred to 0.1 M sodium phosphate buffer and subsequently cut into blocks of approximately 1 mm × 2 mm × 3 mm size. These were post-fixed in aqueous 1% osmium tetroxide for 1 h, washed in several changes of distilled water and then immersed in 0.5% aqueous uranyl acetate for 1 h. The blocks were dehydrated in a series of increasing ethanol concentrations (70%, 90% and twice at 100%), before infiltration with Araldite epoxy resin, using a 1:1 resin:propylene oxide intermediate step, embedded in fresh resin and finally cured in moulds at 60 °C. Ultrathin sections (90 nm thickness) were cut from embedded blocks using an UC6 ultramicrotome (Leica Microsystems) with a diamond knife and collected on copper 200 mesh grids with a formvar support film. They were imaged at 120 kV using the Technai 12 transmission electron microscope (FEI).

Gene expression analysis

Total RNA was extracted with QIAzol Lysis Reagent (Qiagen) and cDNA was synthesized using the SuperScript III First-Strand Synthesis System (Thermo Fisher Scientific). Quantitative PCR was performed using the ABI PRISM 7500 Fast Sequence Detection System (Thermo Fisher Scientific) in accordance with the manufacturer's instructions. A list of the TaqMan probes (Thermo Fisher Scientific) used in the study is provided in Supplementary Table 3. Thermocycling was performed with an initial cycle at 95 °C for 20 s, followed by 45 cycles at 95 °C for 3 s and 60 °C for 30 s. The expression level of human mRNA in rat lacrimal glands was normalized (Extended Data Fig. 9k) using the average of human *GAPDH* expression in lacrimal-gland-like organoids for a matter of practical convenience.

Bulk RNA-seq analysis was performed at the NGS core facility of the Genome Information Research Center at the Research Institute for Microbial Diseases, Osaka University. In brief, cDNA was generated using a Clontech SMART-Seq v4 Ultra Low Input RNA Kit (Takara Clontech), and the cDNA library was prepared using the KAPA Library Preparation Kits (Kapa Biosystems) according to the manufacturer's instructions. Sequencing was performed on an Illumina HiSeq 2500 platform (Illumina) in a 75-base single-end mode. Casava v.1.8.2 was used for base-calling. Sequenced reads were mapped to the human reference genome sequences (hg19) using TopHat v.2.0.13 in combination with Bowtie2 v.2.2.3 and SAMtools v.0.1.19. The fragments per kilobase of exon per million mapped fragments was calculated using Cuffnorm v.2.2.1. The heat map was generated using iDEP software (v.0.90).

scRNA-seq analysis

For scRNA-seq, library preparation was performed using the 10x Genomics Chromium system (10x Genomics). Sequencing was performed at Macrogen Japan using the Truseq library preparation kit and NovaSeq 6000 system (Illumina). Cell Ranger (v.5.0.1)[44] and the DropletUtils package of Bioconductor were used for mapping and filtering the 10x data. Louvain clustering was performed on 11,085 single cells after integrating the three-time-point datasets using the Seurat3 (v.3.2.3)[45] merge function and normalizing the read counts by 'LogNormalize'; npcs = 50, resolution = 1.0. Marker genes were detected using Seurat3 FindMarkers; test.use = wilcox, logfc.threshold = 0.25, adjusted $P < 0.001$. The pseudotime trajectory was analysed using Monocle3 (v.0.2.1.5)[46] by setting cluster 0 of Seurat3 as a root. The Gene Ontology enrichment analysis with a gene set in a cell cluster was conducted using the clusterProfiler package of Bioconductor; pvalueCutoff = 0.01, qvalueCutoff = 0.05, pAdjustMethod = 'BH'. Gene sets that were highly expressed in a cell cluster were detected by hierarchical clustering with averaged gene expression levels. Computational resources were provided by the SHIROKANE supercomputer system at the Human Genome Center of the Institute of Medical Science at the University of Tokyo.

Microarray analysis

The raw microarray datasets were downloaded from NCBI Gene Expression Omnibus (GEO). These comprised eight samples for lacrimal gland (LG) tissues hybridized on the Affymetrix HTA 2.0 Array and HuGene 1.0 ST Array (GSM2390107, GSM2390108, GSM2390109, GSM2390110, GSM2390111, GSM2390112, GSM2390113, GSM2390114), five samples for salivary (parotid) gland (SG) tissues hybridized on the Affymetrix HG-U133 Plus 2.0 Array (GSM997851, GSM997852, GSM997853, GSM997854, GSM997855), eight samples for mammalian gland (MG) breast tissues hybridized on the Affymetrix HG-U133A Array (GSM3538406, GSM3538416, GSM3538426, GSM3538436, GSM3538446, GSM3538456, GSM3538466, GSM3538476). After the background correction was performed with the CEL files of each tissue,

the perfect match probes were retrieved. Probe counts removed the batch effects by ComBat were normalized by conducting quantile normalization. The mean values of the normalized probe count in the dataset of each tissue were calculated. The relative gene expression values were the mean values divided by the mean of *GAPDH* in each tissue. The R packages oligo and sva were used to process the microarray datasets.

Transplantation of lacrimal-gland-like tissue organoids

All animal experimentation was performed in accordance with the ARVO Statement for the Use of Animals in Ophthalmic and Vision Research and was approved by the animal ethics committees of Osaka University. Female F344/NJcl-rnu/rnu rats (that is, nude rats, approximately 100 to 200 g, aged 4 to 12 weeks) were acquired from CLEA Japan. Animals were anaesthetized with an intraperitoneal injection of 0.15 mg kg^{-1} medetomidine hydrochloride (Nippon Zenyaku Kogyo), 2.0 mg kg^{-1} midazolam (Maruishi Pharmaceutical) and 2.5 mg kg^{-1} butorphanol tartrate (Meiji Seika Pharma), after which the exorbital lacrimal gland was removed. The lacrimal-gland-like organoids to be used for the transplantation experiments had been generated from 10 week SEAMs. Either the whole lacrimal gland, or approximately half of the gland, was removed from the left eye of the rat, after which one or five organoids that had been cultured in Matrigel were placed into the rat's lacrimal gland tissue (with Matrigel still present) and the external skin was sutured (Fig. 4a and Extended Data Fig. 8a, b). After surgery, 0.3% ofloxacin ointment (Santen Pharmaceutical) and 0.1% betamethasone sodium phosphate ointment (Shionogi Pharmaceutical) were administrated twice daily. Rats were euthanized and transplanted organoids were extracted at post-operative day 1, week 2 and week 4.

ELISA analysis of lactoferrin and lysozyme

Cultured lacrimal-gland-like organoids and transplanted organoids were immersed in PBS (6 µl per mg tissue) containing a protease inhibitor cocktail (Nacalai Tesque), after which the protein was extracted using the TissueLyser II (Qiagen) system. After centrifugation at 12,000*g* for 10 min, the aqueous phase was examined by ELISA. Human lactoferrin (LTF) and lysozyme (LYZ) were measured using a quantitative sandwich ELISA according to the manufacturer's instructions (LTF, ab200015, Abcam; LYZ, CY-8114, MBL). To detect rat lactoferrin in rat lacrimal gland tissues and tear fluid, a lactoferrin (rat) ELISA kit (BioVision) was used.

Statistics and reproducibility

Images of immunostaining and organoid formation are shown as representative images from the indicated number of biologically independent experiments. The images in Extended Data Fig. 7h are shown as representative images from $n = 2$ technical replicates, and the images in Extended Data Fig. 6g are from $n = 1$ experiment for each of the experimental conditions. All data are expressed as mean ± s.d. Wilcoxon rank-sum tests (two-sided) were performed for two-group comparisons (Fig. 3d and Extended Data Figs. 1i, 5d, 6b and 9j, k). Dunn's tests (Bonferroni-corrected) were performed for multiple comparisons (Figs. 2h, 3j and 4h and Extended Data Figs. 6f and 9i). All statistical analyses were performed using JMP Pro (v.14.0, v.15.0, SAS Institute). Statistical significance was set at $P < 0.05$. Exact P values are provided in the source data.

Reporting summary

Further information on research design is available in the Nature Research Reporting Summary linked to this paper.

Data availability

Bulk RNA-seq and scRNA-seq datasets have been deposited at the NCBI GEO repository under accession numbers GSE157678 and GSE174653. Source data are provided with this paper.

40. Okubo T. et al. Fabrication of three-dimensional lacrimal-gland-like tissue organoids from human pluripotent stem cells. *Protocol Exchange* https://doi.org/10.21203/rs.3.pex-1821/v1 (2022).
41. Nakagawa, M. et al. A novel efficient feeder-free culture system for the derivation4 of human induced pluripotent stem cells. *Sci. Rep.* **4**, 3594 (2014).
42. Yoshimoto, S. et al. Inhibition of Alk signaling promotes the induction of human salivary-gland-derived organoids. *Dis. Model Mech.* **13**, dmm045054 (2020).
43. Leir, S.-H. et al. An organoid model to assay the role of CFTR in the human epididymis epithelium. *Cell Tissue Res.* **381**, 327–336 (2020).
44. Zheng, G. X. et al. Massively parallel digital transcriptional profiling of single cells. *Nat. Commun.* **8**, 14049 (2017).
45. Stuart, T. et al. Comprehensive integration of single-cell data. *Cell* **177**, 1888–1902 (2019).
46. Trapnell, C. et al. The dynamics and regulators of cell fate decisions are revealed by pseudotemporal ordering of single cells. *Nat. Biotechnol.* **32**, 381–386 (2014).

Acknowledgements We thank K. Nomi, T. Soma, K. Maruyama and J. Mantel for technical support and for providing experimental equipment and supporting research grants; D. Okuzaki and the staff at the NGS Core Facility of the Genome Information Research Center at the Research Institute for Microbial Diseases, Osaka University for support in RNA-seq and data analysis; and Y. Honma of ROHTO Pharmaceutical for scientific discussions. This work was supported in part by the Project for the Realization of Regenerative Medicine from The Japan Agency for Medical Research and Development (AMED, JP19bm0404058h0001, JP20bm0404058h0002, JP21bm0404058h0003), Grant-in-Aid for Scientific Research (17K11480, 20H03842) from Japan Society for the Promotion of Science (JSPS) and AMED-CREST (JP20gm1210004h0002, JP21gm1210004h0004).

Author contributions R.H. and T.O. designed the research plan. T.K. performed the PS cell maintenance culture. T.O., Y.K., Y.I., T.I. and T.K. performed the PS cell differentiation culture. Y.K., S.S. and T.O. performed the flow cytometry experiments and lacrimal gland induction. R.H., T.O., Y.K., T.I. and Y.I. performed immunostaining, western blot and gene expression analyses. Y.K. performed swelling assay. K.S. and T.I. performed the ELISAs and animal experiments. R.H., T.O., S.S. and Y.K. analysed the data. Y.I. and Y.K. performed the siRNA experiments. S.-J.P. and R.H. performed the scRNA-seq analysis. R.D.Y., Y.I. and A.J.Q. performed the transmission electron microscopy experiments. S.S., K.N. and A.J.Q. supervised the research. R.H., T.O. and A.J.Q. wrote the manuscript. R.H. and K.N. obtained financial support.

Competing interests R.H. is the holder of an Endowed Chair provided by ROHTO Pharmaceutical. The other authors declare no competing interests.

Additional information

Supplementary information The online version contains supplementary material available at https://doi.org/10.1038/s41586-022-04613-4.

Correspondence and requests for materials should be addressed to Ryuhei Hayashi.

Peer review information *Nature* thanks Karl Koehler and the other, anonymous, reviewer(s) for their contribution to the peer review of this work.

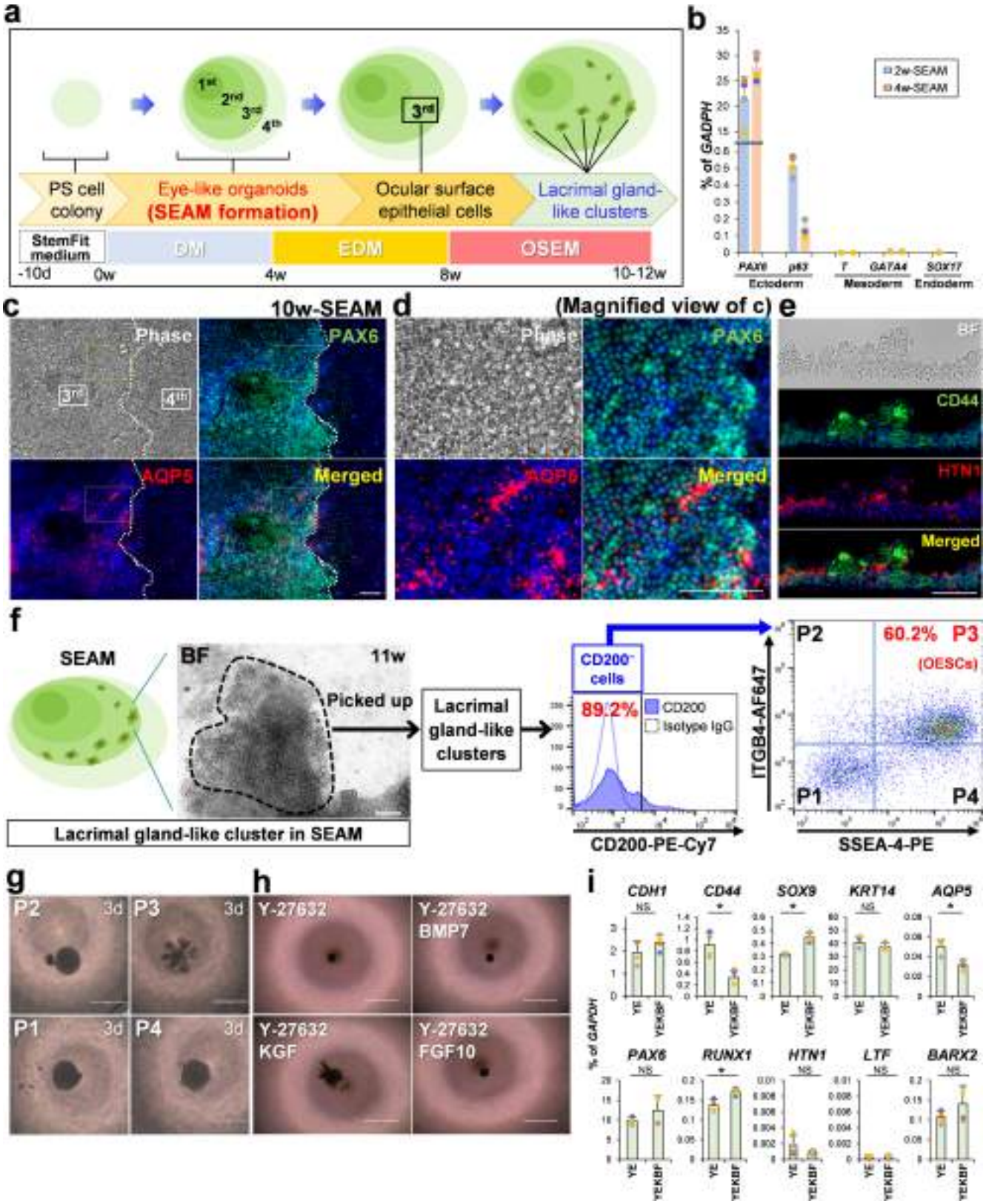

Extended Data Fig. 1 | See next page for caption.

Extended Data Fig. 1 | Differentiation of multiple ocular cell lineages in the SEAM. a, Schematic illustration of the method for inducing lacrimal-gland-like clusters in a SEAM. **b**, Gene expression of three germ layer markers in 2- and 4-week differentiated SEAMs (n = 4 biological replicates). Data are presented as mean ± s.d. **c**–**d**, Immunostaining for PAX6 (green) and AQP5 (red) in a 10-week differentiated SEAM. Magnified views of the dashed areas in (c) are shown in (d). n = 3 distinct samples. Nuclei, blue. Scale bars, 100 µm. **e**, Immunostaining for CD44 (green) and HTN1 (red) in a thin section of lacrimal-gland-like clusters in a 14-week differentiated SEAM. n = 3 biological replicates. BF, bright field; Scale bar, 100 µm. **f**, Flow cytometric analysis of SSEA-4, ITGB4, and CD200 in isolated lacrimal-gland-like clusters induced in SEAMs after 11 weeks of culture. Four populations in the $CD200^-$ cells are categorized as P1–P4. n = 2 biological replicates. Scale bar, 200 µm. OESCs, ocular surface epithelial stem cells. **g**, 3D culture of the sorted cell populations (P1–P4) to induce lacrimal-gland-like organoids at day 3 (n = 3 biological replicates). Scale bars, 1,000 µm. **h**, Screening for organoid induction medium using a combination of lacrimal gland-related cytokines and Y-27632. n = 2 biological replicates. Scale bars, 1,000 µm. **i**, Comparison of lacrimal gland-related gene expression in the organoids cultured in medium containing either Y-27632 and EGF (YE), or Y-27632, EGF, KGF, BMP7 and FGF10 (YEKBF). *$p < 0.05$ (n = 4 biological replicates; NS, not significant). Data are presented as mean ± s.d. Exact p values are provided in the Source Data.

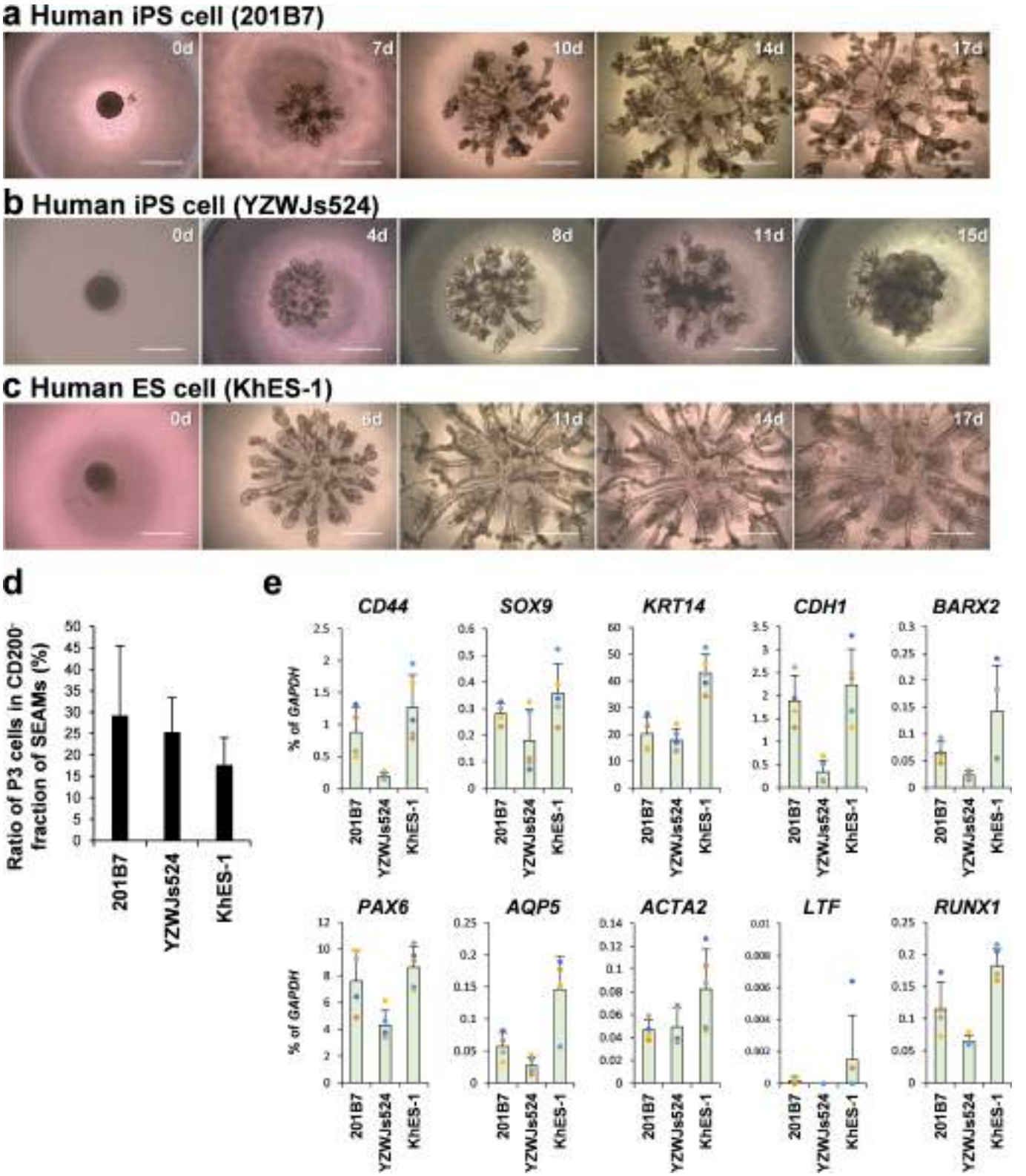

Extended Data Fig. 2 | Formation of lacrimal-gland-like organoids from human iPS cells and ES cells. a–c, Development of lacrimal-gland-like organoids from hiPSC lines 201B7 (a) and YZWJs524 (b), and the human ES cell line, KhES-1 (c). For 201B7, n = 413; for YZWJs524, n = 6; for KhES-1, n = 40 organoids. Scale bars, 1,000 µm. **d**, Ratio of P3 cells in the $CD200^-$ fraction of SEAMs derived from pluripotent stem cell lines; 201B7 (n = 91 biological replicates), YZWJs524 (n = 5 biological replicates), and KhES-1 (n = 10 biological replicates). Data are presented as mean ± s.d. **e**, Gene expression analysis of lacrimal gland markers in lacrimal-gland-like organoids derived from pluripotent stem cell lines, 201B7 (n = 4 biological replicates), YZWJs524 (n = 5 biological replicates), and khES-1 (n = 5 biological replicates). Data are presented as mean ± s.d.

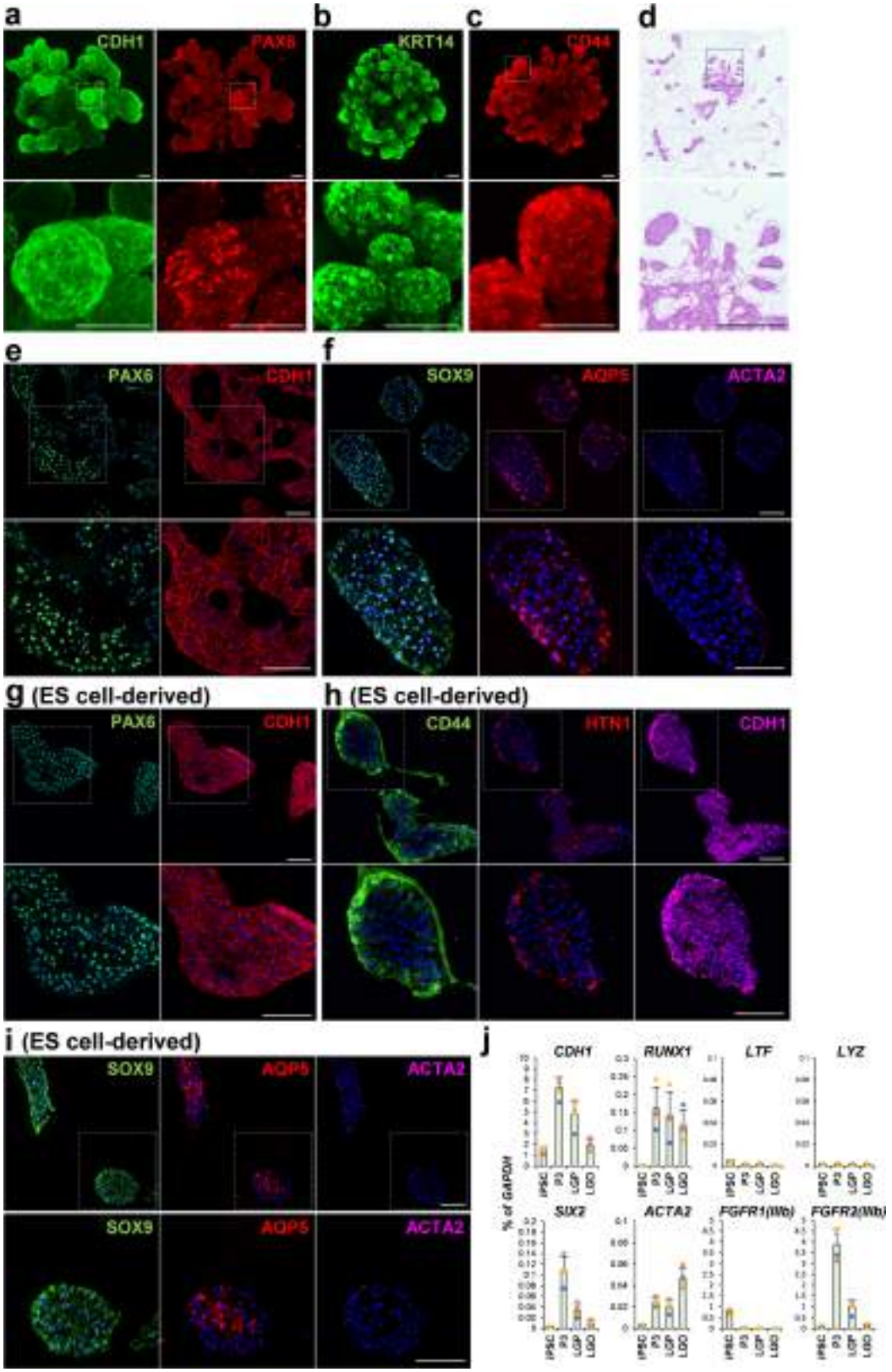

Extended Data Fig. 3 | See next page for caption.

Extended Data Fig. 3 | Characterization of lacrimal-gland-like organoids. **a**–**c**, Light sheet fluorescence microscopy of lacrimal-gland-like organoids stained with CDH1 and PAX6 (a), KRT14 (b) and CD44 (c). Lower panels show magnified views of the upper panels. n = 2 biological replicates. Scale bars, 200 µm. **d**, H&E staining of hiPSC-derived lacrimal-gland-like organoids. n = 3 biological replicates. Scale bars, 500 µm. **e**, Immunolocalization of PAX6 (green) and CDH1 (red) in thin sections of hiPSC-derived lacrimal-gland-like organoids. n = 3 biological replicates. Nuclei, blue. Scale bars, 100 µm. **f**, Immunostaining for SOX9 (green), AQP5 (red) and ACTA2 (magenta) in thin sections of hiPSC-derived lacrimal-gland-like organoids. n = 3 biological replicates. Nuclei, blue. Scale bars, 100 µm. **g**–**i**, Immunostaining of KhES-1-derived lacrimal-gland-like organoids for PAX6 (green) and CDH1 (red) (g), CD44 (green), HTN1 (red) and CDH1 (magenta) (h), and SOX9 (green), AQP5 (red) and ACTA2 (magenta) (i). n = 3 biological replicates. Nuclei, blue. Scale bars, 100 µm. **j**, Gene expression analysis for lacrimal gland-related markers in iPS cells (iPSC), P3 cells, lacrimal-gland-like progenitors (LGP) and organoids (LGO). n = 4 biological replicates. Data are presented as mean ± s.d.

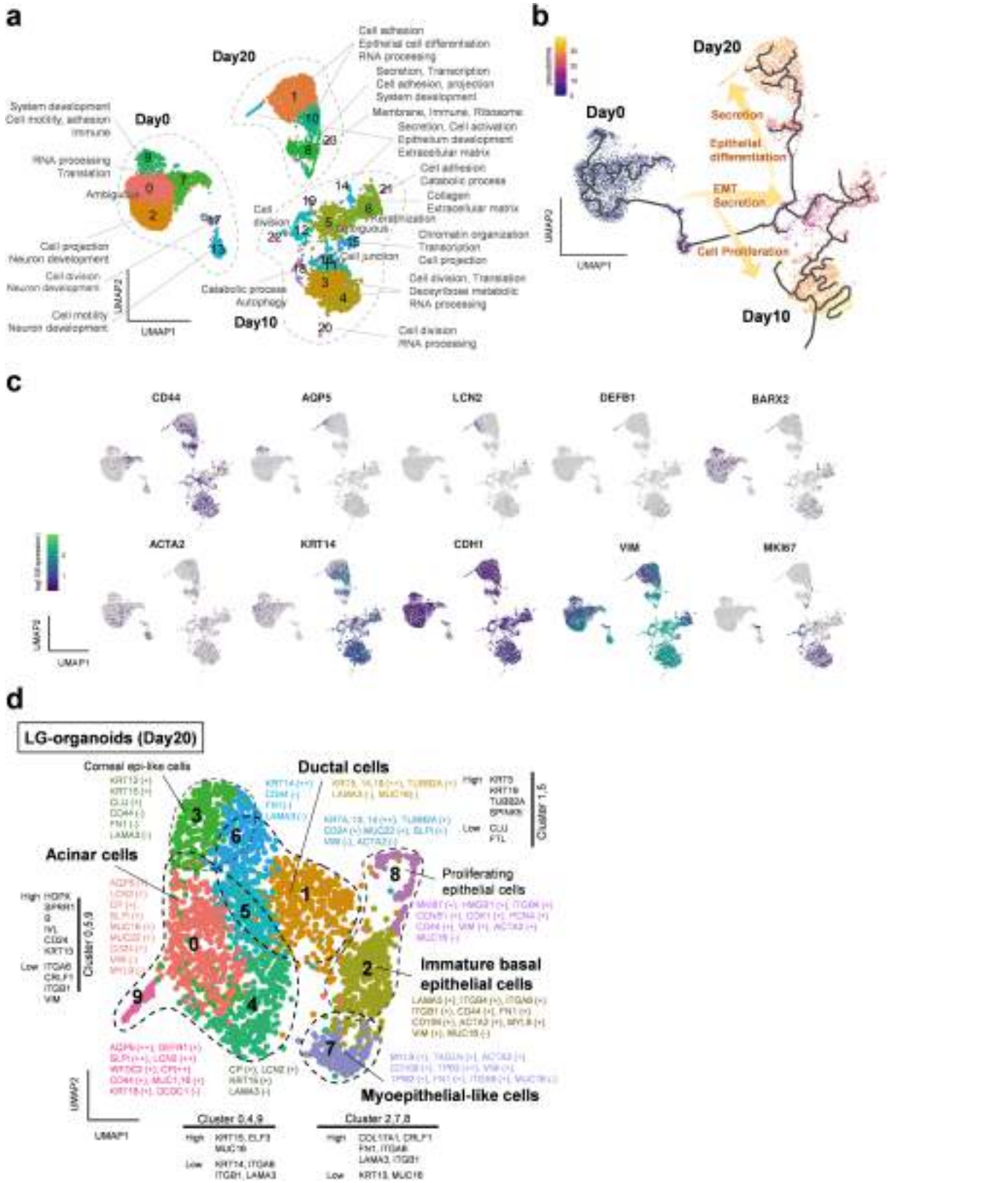

Extended Data Fig. 4 | Characterization of iPS cell-derived lacrimal-gland-like organoids by single-cell RNA sequencing. a, Uniform manifold approximation and projection (UMAP) plot of all single cells and the summary of enriched GO terms in each cluster; n = 4071 cells (day 0), n = 4566 cells (day 10), n = 2448 cells (day 20). **b**, Pseudotime trajectory of the single-cell transcriptome showing three branches from the root (cluster 0 of day 0). These represent active epithelial-mesenchymal transition (EMT), cell proliferation, and the development of epithelial secretory cells. **c**, Cell populations preferentially expressed lacrimal gland-related genes. **d**, Cell-type annotations of lacrimal-gland-like organoids (day 20) with positive and negative marker genes.

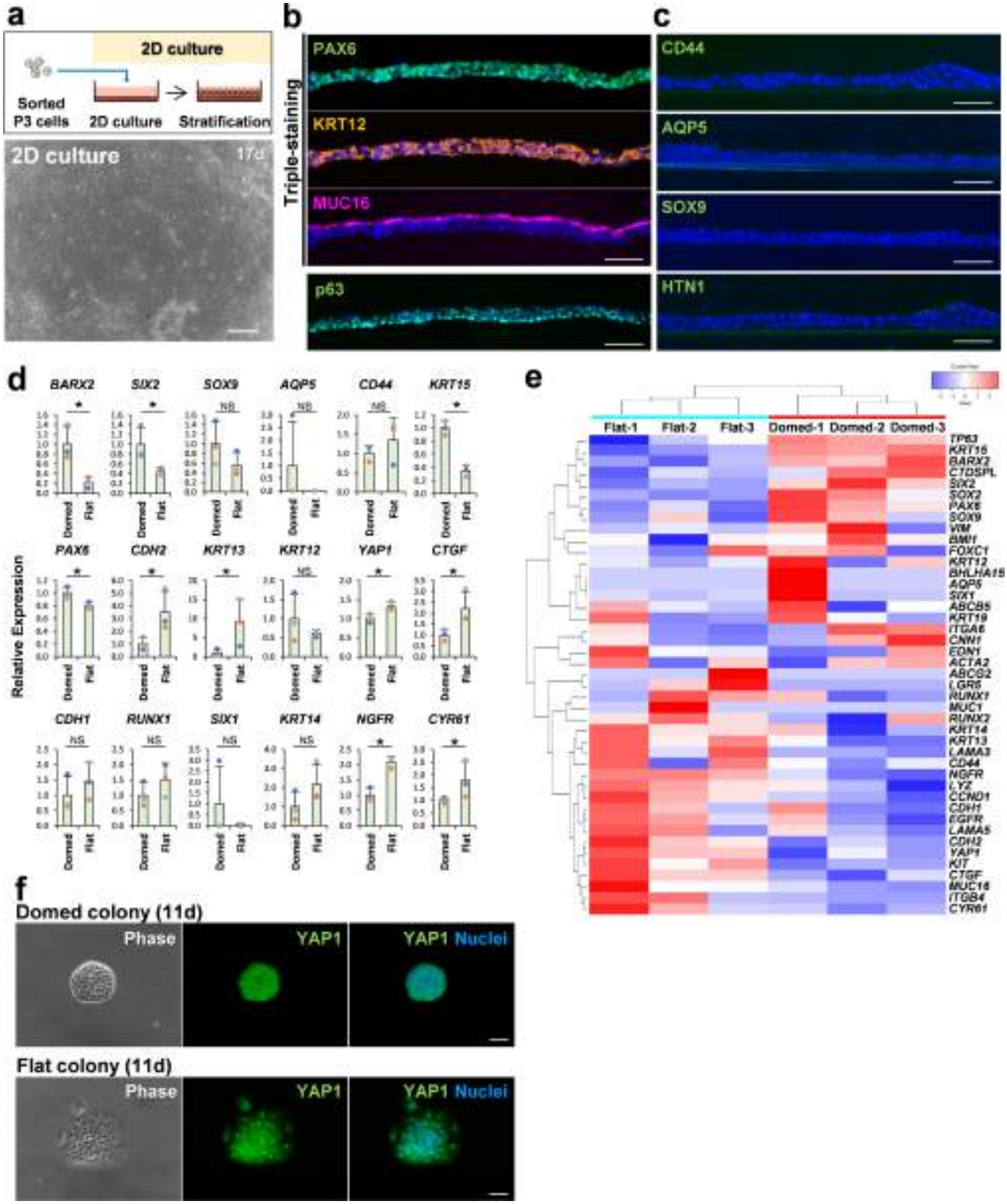

Extended Data Fig. 5 | Characterization of domed and flat colonies derived from ocular surface epithelial stem cells. a–**c**, Corneal epithelial differentiation from P3-ocular surface epithelial stem cells by 2D culture (a), along with immunostaining for corneal epithelial (b) and lacrimal gland markers (c) in the epithelial cell sheet. Nuclei, blue; n = 3 biological replicates; Scale bars, 100 μm. **d**, Gene expression analysis for lacrimal gland-related markers in domed and flat colonies. Expression in domed colonies is shown as 1.0. *$p < 0.05$ (n = 3 distinct colonies from one experiment for each experimental condition; NS, not significant). Data are presented as mean ± s.d. Exact p values are provided in the Source Data. **e**, A cluster heatmap based on the expression of lacrimal gland, epithelial cell and YAP-related genes. **f**, Immunostaining for YAP1 (green) in domed (upper panels) and flat (lower panels) colonies derived from sorted P3 cells. n = 3 biological replicates. Nuclei, blue. Scale bars, 100 μm.

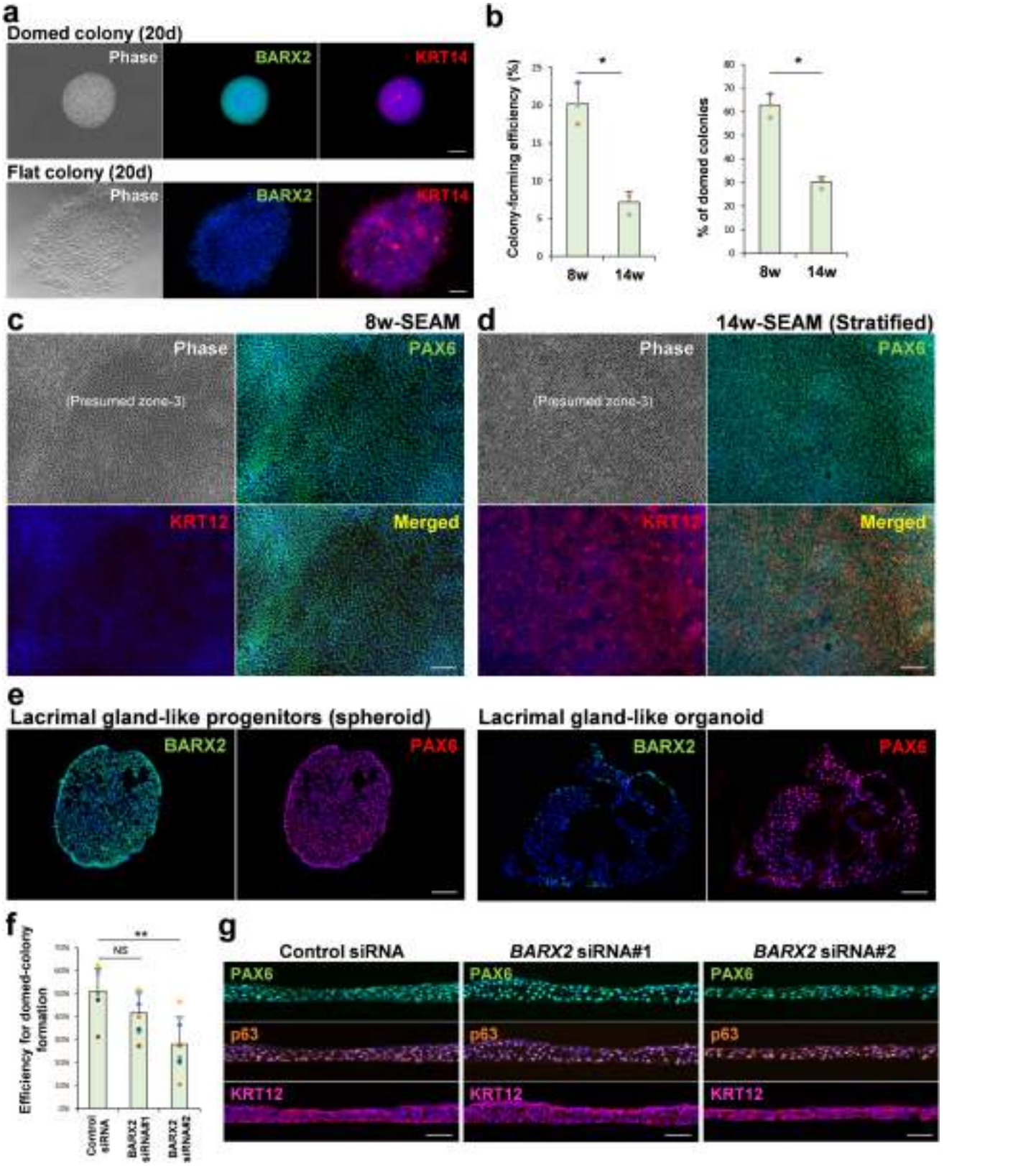

Extended Data Fig. 6 | See next page for caption.

Extended Data Fig. 6 | The involvement of BARX2 in lacrimal-gland-like organoid formation. a, Immunostaining for BARX2 (green) and KRT14 (red) in domed (upper panels) and flat (lower panels) colonies derived from sorted P3 cells. n = 3 biological replicates. Nuclei, blue. Scale bars, 100 μm. **b**, Colony-forming efficiency and the proportion (at day 21) of domed colonies of P3 cells sorted from SEAMs after 8 and 14 weeks of differentiation culture. n = 3 biological replicates. Data are presented as mean ± s.d. Exact p values are provided in the Source Data. **c**–**d**, Immunostaining for PAX6 (green) and KRT12 (red) in 8-week (c) and 14-week (d) differentiated SEAMs. n = 3 biological replicates. Nuclei, blue. Scale bars, 100 μm. **e**, Immunostaining for BARX2 (green) and PAX6 (red) in lacrimal-gland-like progenitors (left panels) and organoids (right panels). n = 3 biological replicates. Nuclei, blue. Scale bars, 100 μm. **f**, Effect of BARX2 knockdown using siRNA on domed-colony formation. *$p < 0.01$ (n = 8 biological replicates; NS, not significant). Data are presented as mean ± s.d. Exact p values are provided in the Source Data. **g**, Effect of BARX2 knockdown using siRNA on corneal epithelial differentiation. n = 1 sample for each experimental condition. Nuclei, blue, Scale bars, 100 μm.

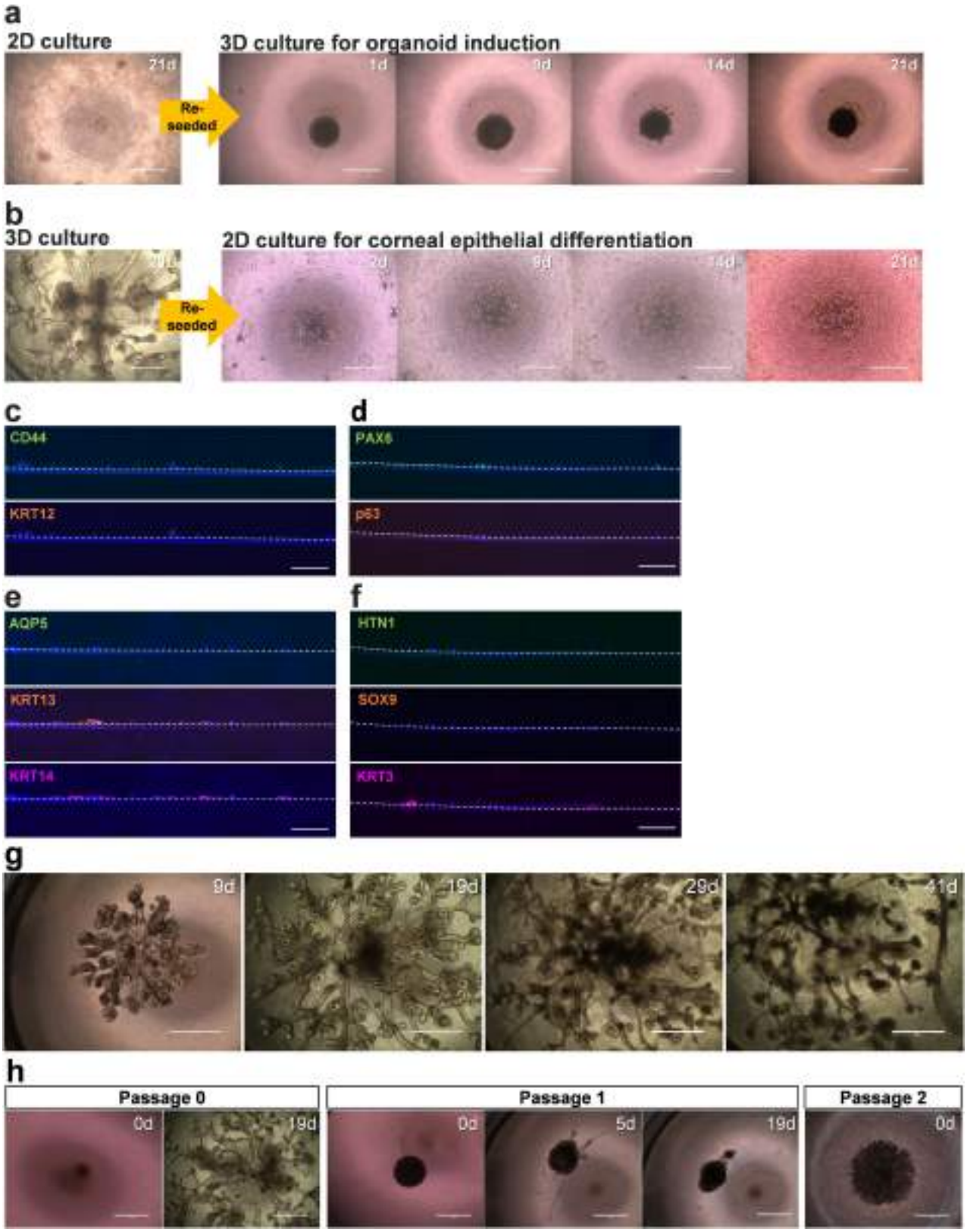

Extended Data Fig. 7 | Differentiation capability of SEAM-derived lacrimal-gland-like organoids and corneal epithelial cell sheets. a, 3D organoid culture using cells from SEAM-derived corneal epithelial cells. n = 8 biological replicates. Scale bars, 1,000 µm. **b**, 2D corneal epithelial culture using cells from lacrimal-gland-like organoids. n = 19 biological replicates. Scale bars, 1,000 µm. **c**–**f**, Immunostaining of cells derived from lacrimal-gland-like organoids after 2D cultivation as shown in (b): (c) CD44 (green) and KRT12 (orange); (d) PAX6 (green) and p63 (orange); (e) AQP5 (green), KRT13 (orange), and KRT14 (magenta); (f) HTN1 (green), SOX9 (orange), and KRT3 (magenta). n = 3 biological replicates in (c) - (f). Nuclei, blue. Scale bars, 100 µm. **g**, Prolonged 3D cultivation of lacrimal-gland-like organoids up to 41 days. n = 2 biological replicates. Scale bars, 1,000 µm. **h**, Cell passaging of lacrimal-gland-like organoids. n = 2 technical replicates. Scale bars, 1,000 µm.

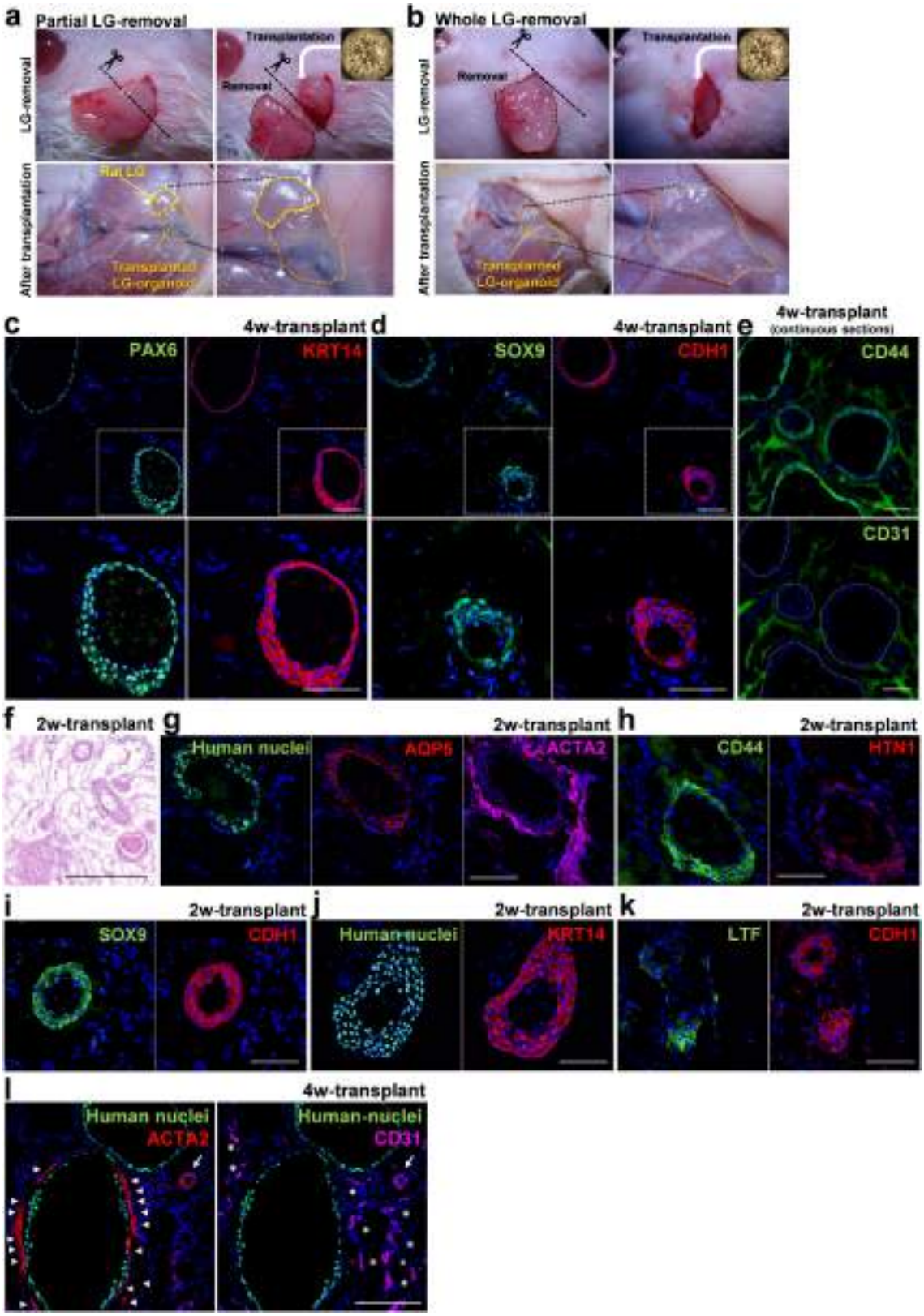

Extended Data Fig. 8 | See next page for caption.

Extended Data Fig. 8 | Transplanted lacrimal-gland-like organoids. **a**–**b**, Images depicting (a) partial and (b) whole removal of rat lacrimal gland and transplantation of lacrimal-gland-like organoids. Scale bar (inset images), 1,000 μm. **c**–**e**, Immunostaining for (c) PAX6 (green) and KRT14 (red), (d) SOX9 (green) and CDH1 (red), and (e) CD44 and CD31 (green) in serial sections of grafted lacrimal-gland-like organoids (5×) four weeks after transplantation into rat lacrimal glands. Lower panels in (c-d) show magnified views of the upper panels. Dotted lines in (e) indicate $CD44^+$ lacrimal gland cells. n = 3 biological replicates. Nuclei, blue. Scale bars, 100 μm. **f**, H&E staining of 2 week-transplanted tissue. n = 3 biological replicates. Scale bar, 500 μm. **g**–**k**, Immunostaining of grafted lacrimal-gland-like organoids (5×) two weeks following transplantation to rat lacrimal glands: (g) human nuclei (green), AQP5 (red) and ACTA2 (magenta); (h) CD44 (green) and HTN1 (red); (i) SOX9 (green) and CDH1 (red); (j) human nuclei (green) and KRT14 (red); (k) LTF (green) and CDH1 (red), n = 3 biological replicates. Nuclei, blue; Scale bars, 100 μm. **l**, Immunostaining of human nuclei (green), ACTA2 (red) and CD31 (magenta) in grafted lacrimal-gland-like organoids four weeks after transplantation into rat lacrimal glands. Arrowheads indicate stromal cells, asterisks indicate vascular endothelial cells, and short arrows indicate blood vessels. n = 3 biological replicates. Nuclei, blue. Scale bars, 100 μm.

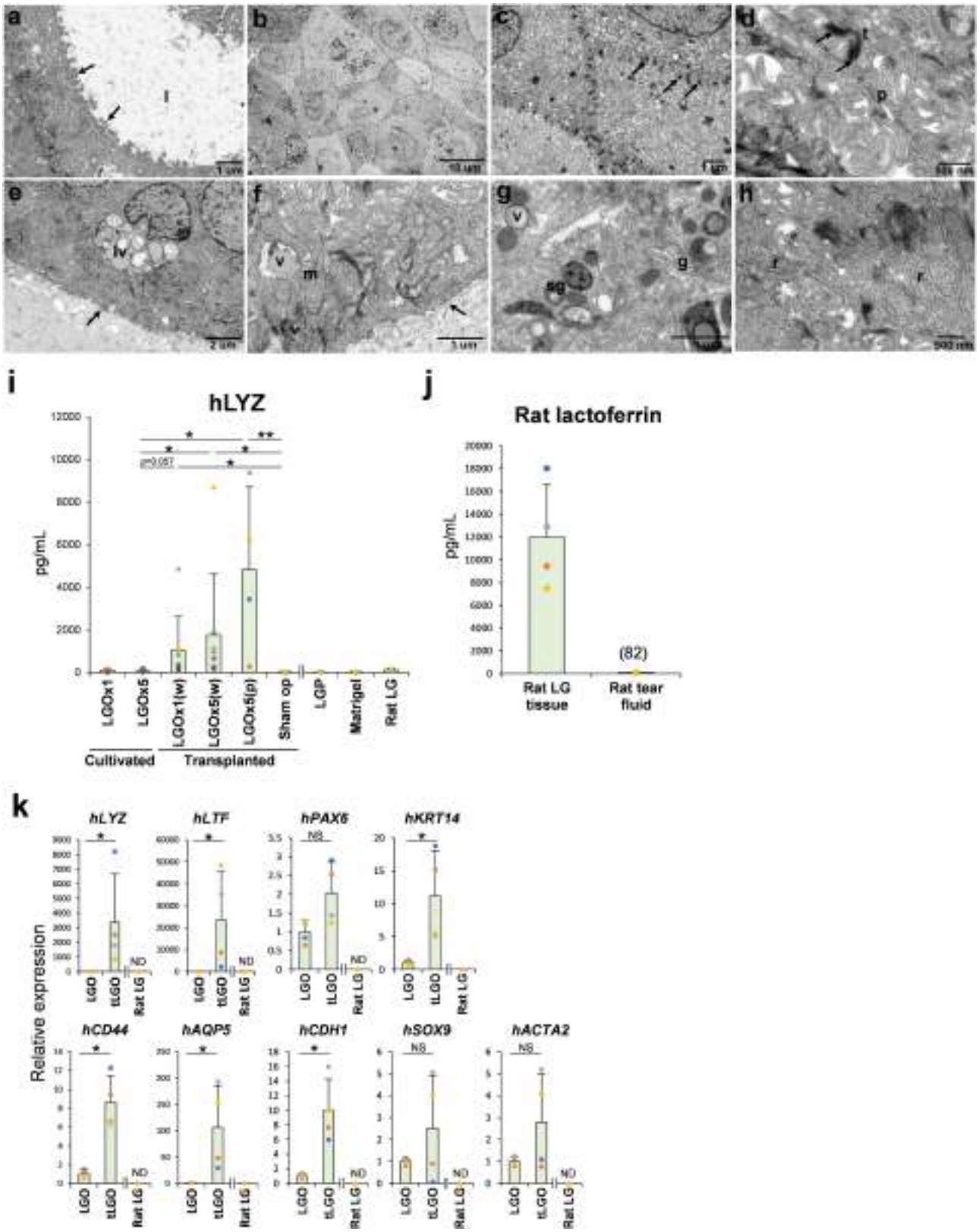

Extended Data Fig. 9 | See next page for caption.

Extended Data Fig. 9 | Transmission electron microscopy and ELISA of transplanted lacrimal-gland-like organoids. Transmission electron microscopy of human iPS cell-derived lacrimal-gland-like organoids after 4 weeks of transplantation. **a**, lumen (l) and lining cells with numerous microvilli (arrows). **b**, variable basophilia of secretory acinar cells peripheral to lumen. **c**, multiple desmosomes (arrows) are located along membranes between adjacent secretory cells. **d**, lateral membranes of secretory cells express interdigitating finger-like processes (p) and tonofilaments (t) associated with desmosomes (arrows). **e**, lipid vesicle inclusions (lv) are present within basal secretory cells, which rest on a basement membrane (arrow). **f**, clusters of mitochondria (m) and a lipid droplet (v) in the cytoplasm of a basal acinar cell, adjacent to multi-layered basal lamina (arrow). **g**, acinar cells towards lumen exhibit secretory granules (sg) with variable size and density, lipid droplets (v) and extensive Golgi bodies (g). **h**, regions of rough-surfaced endoplasmic reticulum (r) are also present. n = 2 biological replicates in (a) - (h). **i**, ELISA for human lysozyme (hLYZ) in lacrimal-gland-like organoids (LGOs). (w) and (p) indicate whole and partial lacrimal gland-removal surgeries, respectively. $^{*}p < 0.05$, $^{**}p < 0.01$ (LGO×1, LGO×5, LGO×1 (w) and LGO×5 (w), n = 8. Others, n = 4 biological replicates). Data are presented as mean ± s.d. Exact p values are provided in the Source Data. **j**, ELISA for rat lactoferrin in lacrimal gland tissues and tear fluid. n = 4 biological replicates. Data are presented as mean ± s.d. **k**, Expression of lacrimal gland-related genes in lacrimal-gland-like organoids (LGOs), transplanted organoids (tLGO), and rat lacrimal gland (Rat LG). The expression level in the LGO is shown to be 1.0. $^{*}p < 0.05$ (n = 4 biological replicates; NS, not significant). Data are presented as mean ± s.d. Exact p values are provided in the Source Data. ND, not detected.

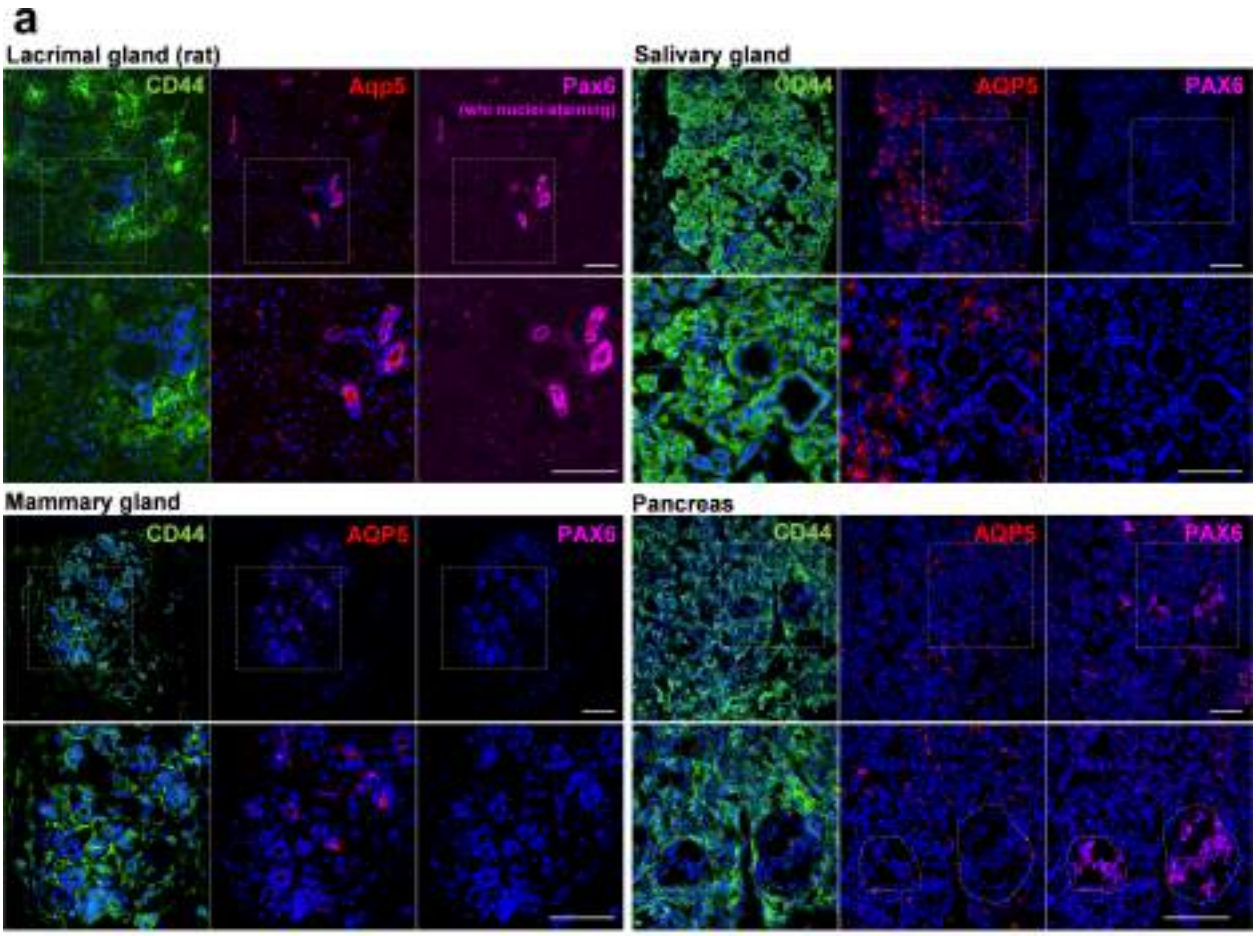

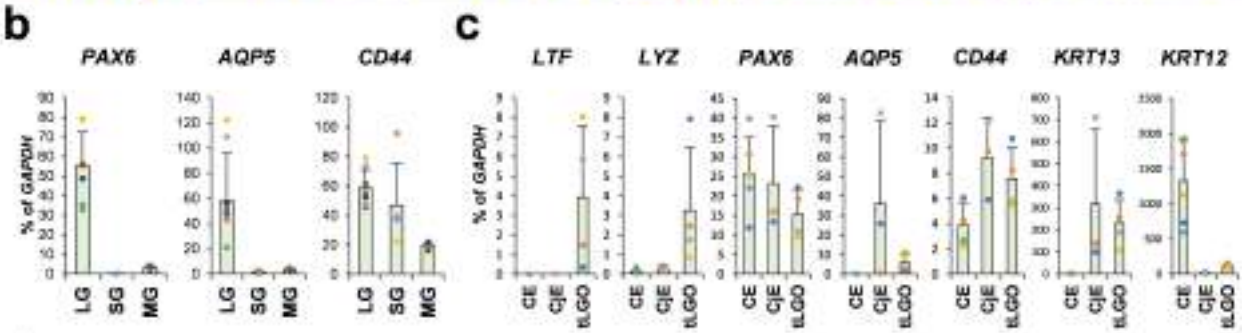

d

Markers	iPS cell-tLGO	LG	SG	MG	CE	CjE	PC	
							Exocrine	Islet
PAX6	+	+	-	-	+	+	-	+
AQP5	+	+	+	+	-	+	+	-
CD44	+	+	+	+	+	+	+	-
LTF/LYZ	+	(ND)	(ND)	(ND)	-	-	(ND)	(ND)

Extended Data Fig. 10 | See next page for caption.

Extended Data Fig. 10 | Comparison of exocrine gland cells. **a**, Immunostaining for CD44 (green), AQP5 (red) and PAX6 (magenta) in lacrimal gland (rat), salivary gland, mammary gland and pancreas (all humans). Lower panels show magnified views of the upper panels. Dotted lines in pancreas tissue indicate the presumptive region of islets. n = 3 biological replicates (rat lacrimal gland) and n = 1 (human gland tissue). Nuclei, blue. Scale bars, 100 μm. **b**, Expression of *PAX6*, *AQP5* and *CD44* in human exocrine gland tissues, lacrimal glands (n = 8), salivary glands (n = 5), and mammary glands (n = 8) based on existing microarray datasets. **c**, Expression of lacrimal gland and ocular surface epithelium-related genes in transplanted lacrimal-gland-like organoids (tLGO) and in human corneal and conjunctival epithelial cells. CE, corneal epithelial cell; CjE, conjunctival epithelial cell. tLGO, n = 4; CE, n = 6; CjE, n = 3 biological replicates. Data are presented as mean ± s.d. **d**, Summary of expression of lacrimal gland-related markers in glandular tissues and ocular surface epithelium. Data indicate that PAX6, AQP5, LTF and LYZ-expressing cells are lacrimal gland type cells. SG, salivary gland; MG, mammary gland; PC, pancreas; ND, not determined.

nature research

Corresponding author(s): Ryuhei HAYASHI

Last updated by author(s): Dec 28th, 2021

Reporting Summary

Nature Research wishes to improve the reproducibility of the work that we publish. This form provides structure for consistency and transparency in reporting. For further information on Nature Research policies, see our Editorial Policies and the Editorial Policy Checklist.

Statistics

For all statistical analyses, confirm that the following items are present in the figure legend, table legend, main text, or Methods section.

n/a	Confirmed	
☐	☒	The exact sample size (*n*) for each experimental group/condition, given as a discrete number and unit of measurement
☐	☒	A statement on whether measurements were taken from distinct samples or whether the same sample was measured repeatedly
☐	☒	The statistical test(s) used AND whether they are one- or two-sided *Only common tests should be described solely by name; describe more complex techniques in the Methods section.*
☒	☐	A description of all covariates tested
☐	☒	A description of any assumptions or corrections, such as tests of normality and adjustment for multiple comparisons
☐	☒	A full description of the statistical parameters including central tendency (e.g. means) or other basic estimates (e.g. regression coefficient) AND variation (e.g. standard deviation) or associated estimates of uncertainty (e.g. confidence intervals)
☐	☒	For null hypothesis testing, the test statistic (e.g. *F*, *t*, *r*) with confidence intervals, effect sizes, degrees of freedom and *P* value noted *Give P values as exact values whenever suitable.*
☒	☐	For Bayesian analysis, information on the choice of priors and Markov chain Monte Carlo settings
☒	☐	For hierarchical and complex designs, identification of the appropriate level for tests and full reporting of outcomes
☒	☐	Estimates of effect sizes (e.g. Cohen's *d*, Pearson's *r*), indicating how they were calculated

Our web collection on statistics for biologists contains articles on many of the points above.

Software and code

Policy information about availability of computer code

Data collection	For Bulk RNA sequencing, sequencing data was obtained using the Illumina HiSeq 2500 platform in 75-base single-end mode with Illumina Casava software (ver. 1.8.2). For single-cell RNA sequencing, library preparation was performed using the 10x Genomics Chromium system (10x Genomics, Pleasanton, CA, USA). Sequencing was performed at Macrogen Japan (Tokyo, Japan) with the Truseq library preparation kit and NovaSeq 6000 (Illumina).

Data analysis	For Bulk RNA sequencing, sequenced reads were mapped to the human reference genome sequences (hg19) using TopHat software (ver. 2.0.13) in combination with Bowtie2 (ver. 2.2.3) and SAMtools (ver.0.1.19) software. The fragments per kilobase of exon per million mapped fragments (FPKMs) was calculated using Cuffnorm software (ver. 2.2.1.). The heatmap was generated using iDEP software (ver.0.90). For single-cell RNA sequencing, Cell Ranger (ver. 5.0.1) and the DropletUtils package of Bioconductor were used for mapping and filtering the 10x data. Louvain clustering was performed on 11,085 single cells after integrating the 3-time point datasets using the Seurat3 (ver. 3.2.3) "merge" function and normalising the read counts by "LogNormalize"; npcs = 50, resolution = 1.0. Marker genes were detected using Seurat3 "FindMarkers"; test.use = wilcox, logfc.threshold = 0.25, adjusted p-value < 0.001. The pseudotime trajectory was analysed by Monocle3 (ver. 0.2.1.5) by setting Cluster 0 of Seurat3 as a root. The Gene-Ontology (GO) enrichment analysis with a gene set in a cell cluster was conducted using the clusterProfiler package of Bioconductor; pvalueCutoff = 0.01, qvalueCutoff = 0.05, pAdjustMethod = "BH". Gene sets that were highly expressed in a cell cluster were detected by hierarchical clustering with averaged gene expression levels. Flow cytometry data were analysed using SH800 software (Cell Sorter Software, ver.2.15, Sony corporation, Tokyo, Japan) and FlowJo programs (Ver. 10.61, TreeStar, San Carlos, CA, USA). Three dimensional microscopic images were obtained by light sheet microscopy and analysed by Imaris software ver. 6 (Zeiss, Jena, Germany). All statistical analyses were performed using the JMP Pro software program (ver. 14.0, 15.0, SAS institute Inc, Cary, North Carolina, US).

For manuscripts utilizing custom algorithms or software that are central to the research but not yet described in published literature, software must be made available to editors and reviewers. We strongly encourage code deposition in a community repository (e.g. GitHub). See the Nature Research guidelines for submitting code & software for further information.

Data

Policy information about availability of data

All manuscripts must include a data availability statement. This statement should provide the following information, where applicable:

- Accession codes, unique identifiers, or web links for publicly available datasets
- A list of figures that have associated raw data
- A description of any restrictions on data availability

RNA-seq datasets are deposited in the GEO repository under accession code GSE157678 and GSE174653. Other datasets generated during and/or analysed during the current study are available from the corresponding author on reasonable request.
Regarding publicly available dataset, the raw microarray datasets were downloaded from NCBI GEO. These comprised 8 samples for lacrimal gland (LG) tissues hybridized on Affymetrix HTA 2.0 Array and HuGene 1.0 ST Array (GSM2390107, GSM2390108, GSM2390109, GSM2390110, GSM2390111, GSM2390112, GSM2390113, GSM2390114), 5 samples for salivary (parotid) gland (SG) tissues hybridized on Affymetrix HG-U133 Plus 2.0 Array (GSM997851, GSM997852, GSM997853, GSM997854, GSM997855), 8 samples for mammalian gland (MG) breast tissues hybridized on Affymetrix HG-U133A Array (GSM3538406, GSM3538416, GSM3538426, GSM3538436, GSM3538446, GSM3538456, GSM3538466, GSM3538476).

Field-specific reporting

Please select the one below that is the best fit for your research. If you are not sure, read the appropriate sections before making your selection.

☒ Life sciences ☐ Behavioural & social sciences ☐ Ecological, evolutionary & environmental sciences

For a reference copy of the document with all sections, see nature.com/documents/nr-reporting-summary-flat.pdf

Life sciences study design

All studies must disclose on these points even when the disclosure is negative.

Sample size	Sample sizes were determined based on previously published works below and preliminary studies though no specific method was used. 1. Fujihara T, Murakami T, Fujita H, Nakamura M, Nakata K. Improvement of corneal barrier function by the P2Y(2) agonist INS365 in a rat dry eye model. Invest Ophthalmol Vis Sci. 2001 Jan;42(1):96-100. 2. Skrzypecki J, Tomasz H, Karolina C. Variability of Dry Eye Disease Following Removal of Lacrimal Glands in Rats. Adv Exp Med Biol. 2019;1153:109-115. 3. Hirayama M, Ogawa M, Oshima M, Sekine Y, Ishida K, Yamashita K, Ikeda K, Shimmura S, Kawakita T, Tsubota K, Tsuji T. Functional lacrimal gland regeneration by transplantation of a bioengineered organ germ. Nat Commun. 2013;4:2497. 4. Joossen C, Lanckacker E, Zakaria N, Koppen C, Joossens J, Cools N, De Meester I, Lambeir AM, Delputte P, Maes L, Cos P. Optimization and validation of an existing, surgical and robust dry eye rat model for the evaluation of therapeutic compounds. Exp Eye Res. 2016 May;146:172-178.
Data exclusions	No samples and animals were excluded from analysis.
Replication	Date reproducibility were confirmed by doing the same experiment more than two times.
Randomization	No specific method of randomization was used, however, for transplantation experiments, female nude rats were allocated into each group at random.
Blinding	The investigators were not blinded to the group allocation in the transplantation experiments. To maximize the objectivity, different individuals performed the transplantations and the examination of the transplants.

Reporting for specific materials, systems and methods

We require information from authors about some types of materials, experimental systems and methods used in many studies. Here, indicate whether each material, system or method listed is relevant to your study. If you are not sure if a list item applies to your research, read the appropriate section before selecting a response.

Materials & experimental systems

n/a	Involved in the study
[ ]	[x] Antibodies
[ ]	[x] Eukaryotic cell lines
[x]	[ ] Palaeontology and archaeology
[ ]	[x] Animals and other organisms
[x]	[ ] Human research participants
[x]	[ ] Clinical data
[x]	[ ] Dual use research of concern

Methods

n/a	Involved in the study
[x]	[ ] ChIP-seq
[ ]	[x] Flow cytometry
[x]	[ ] MRI-based neuroimaging

Antibodies

Antibodies used

KRT12, sc-17098, lot: C0415 (Santa Cruz Biotechnology)
HCAM (CD44), sc-7297, lot: B0516 (Santa Cruz Biotechnology)
p63, sc-8431, lot: AD313 (Santa Cruz Biotechnology)
SOX9, sc-20095, lot: H0715 (Santa Cruz Biotechnology)
AQP5, sc-9890 lot: K2414 (Santa Cruz Biotechnology)
BARX2, sc-9128, lot: K0304 (Santa Cruz Biotechnology)
BARX2, HPA068414, lot: R100282 (Atlas antibodies)
Histatin1, sc-28110, lot: G2610 (Santa Cruz Biotechnology)
E-cadherin, sc-7870, lot: C2508 (Santa Cruz Biotechnology)
E-cadherin, MAB1838, lot: JAT0219041 (R&D)
CHX10, sc-21690, lot: H0614 (Santa Cruz Biotechnology)
KRT14, 905304, lot: B277928 (Biolegend)
KRT14, ab9220, lot: GR221975-17 (Abcam)
PAX6, 901301, lot: B201255 (Biolegend)
PAX6, sc-53108, lot: C1519 (Santa Cruz Biotechnology)
ACTA2, ab7817, lot: GR3257713-3 (Abcam)
KRT13, ab16112, lot: GR2864-20 (Abcam)
Lamin A+C, ab108595, lot: GR257223-26 (Abcam)
α-Crystalline, lot: ADI-SPA-224-F (Enzo Life Sciences)
PE-SSEA-4, 330406, lot: B298578 (Biolegend)
PE-Cy7-CD200, 624052 lot: 0028374 (BD Biosciences)
AF647-CD104 (ITGB4), 624024, lot: 0030325 (BD Biosciences)
PE-IgG3 k (Isotype control), 401320, lot: B257098 (Biolegend)
AF647 IgG1 k (Isotype control), 565571, lot: 9080944 (BD Biosciences)
PE-Cy7-IgG1 k (Isotype control), 557872 lot: 9074806 (BD Biosciences)
MUC16, ab693, lot: GR105598-2 (Abcam)
PECAM-1, M0823, lot: 20049471 (Dako)
YAP, sc-101199, lot: L2717 (Santa Cruz Biotechnology)
LTF, ab158111, lot: GR8396 (Abcam)
ACTB, A5441, lot: 026M4478OV (SIGMA-ALDRICH)

Validation

All primary antibodies were validated using the tissue or cellular samples which are already known to express the proteins of interest.
For KRT12, p63, E-cadherin, KRT14, PAX6, Lamin A+C, YAP, MUC16, ACTA2, SOX9 and KRT13 antibodies, the staining was confirmed on the sections of human corneal scleral tissues as positive control by immunostaining. For AQP5, histatin-1 and CD44 antibodies, the staining was confirmed on the sections of the human gland tissues (CD44, histatin-1 and AQP5) or rat lacrimal gland (CD44 and AQP5) as positive control by immunostaining. For α-Crystalline, CHX10 and BARX2 (sc-53177) antibodies, the staining was confirmed using differentiated human PSC colonies (SEAMs) by immunostaining as shown in the previous reports (For α-Crystalline and CHX10 staining; Hayashi R, et al. Co-ordinated ocular development from human iPS cells and recovery of corneal function. Nature. 2016 Mar 17;531(7594):376-80., for BARX2 staining; Ma J, et al. BARX2 expression is downregulated by CpG island hypermethylation and is associated with suppressed cell proliferation and invasion of gastric cancer cells. Oncol Rep. 2020 Jun;43(6):1805-1818.)
For fluorescent probe-conjugated SSEA-4, CD200, CD104 and the corresponding isotype control antibodies, the staining were confirmed for human PSC-derived corneal epithelial cells by FACS as previously shown (Hayashi R, et al. Co-ordinated ocular development from human iPS cells and recovery of corneal function. Nature. 2016 Mar 17;531(7594):376-80., Hayashi R, et al. CD200 facilitates the isolation of corneal epithelial cells derived from human pluripotent stem cells. Sci Rep. 2018 Nov 8;8(1):16550.
For BARX2 (HPA068414) and ACTB antibodies used in western blotting experiments, the signals were confirmed by the appropriate electrophoresis position (40 and 42 kD, respectively) using cell lysis from human PSC-derived lacrimal gland cells by western blotting.

Eukaryotic cell lines

Policy information about cell lines

Cell line source(s)	Human iPS cell lines, 201B7 and human ES cell line, KhES-1 (RIKEN BioResource Center, Tsukuba, Japan) and YZWJs524 (Kyoto University's Center for iPS Cell Research and Application, Kyoto, Japan)
Authentication	Each pluripotent stem cell line was routinely examined by cell morphology, doubling time and colony-forming efficiency, and on a timely basis by the expression of pluripotent stem cell markers such as OCT3/4, NANOG and TRA-1-60. The use of human ES cells was reviewed and approved by the Ministry of Education, Culture, Sports, Science, and Technology of Japan.
Mycoplasma contamination	Human iPS cell lines (201B7 and YZWJs524) and human ES cell line, KhES-1 were identified as Mycoplasma negative by the provider and by our regular inspections using a PCR-based method employing the e-MycoTM Mycoplasma PCR Detection Kit (# 25235, iNtRON Biotechnology, Seongnam, Korea).
Commonly misidentified lines (See ICLAC register)	We used no commonly misidentified cell lines registered in the ICLAC in this study.

Animals and other organisms

Policy information about studies involving animals; ARRIVE guidelines recommended for reporting animal research

Laboratory animals	Rats, F344/NJcl-rnu/rnu rats, Female, 4-12 weeks old
Wild animals	No wild animals were used in the study.
Field-collected samples	No field collected samples were used in the study.
Ethics oversight	All animal experimentation was performed in accordance with the ARVO Statement for the Use of Animals in Ophthalmic and Vision Research and was approved by the animal ethics committee of Osaka University.

Note that full information on the approval of the study protocol must also be provided in the manuscript.

Flow Cytometry

Plots

Confirm that:

☒ The axis labels state the marker and fluorochrome used (e.g. CD4-FITC).

☒ The axis scales are clearly visible. Include numbers along axes only for bottom left plot of group (a 'group' is an analysis of identical markers).

☒ All plots are contour plots with outliers or pseudocolor plots.

☒ A numerical value for number of cells or percentage (with statistics) is provided.

Methodology

Sample preparation	For lacrimal gland-like culture, after 10 to 12 weeks of differentiation culture using the SEAM method, cells were harvested by Accutase (Thermo Fisher Scientific). Dissociated cells were stained with Alexa-Fluor 647 (AF647)-conjugated anti-ITGB4 (450-9D, BD Biosciences, San Jose, CA, USA), PE-conjugated anti-SSEA-4 (MC813-70, Biolegend, San Diego, CA, USA), and PE-Cy7-conjugated anti-CD200 antibodies (OX-104, BD Biosciences) for one hour on ice. Isotype antibodies corresponding to each antibody were used in control experiments.
Instrument	SH-800, Sony Biotechnology Inc., Tokyo, Japan
Software	SH-800 software (Cell Sorter Software, ver. 2.15, Sony corporation, Tokyo, Japan) and FlowJo software programs (ver. 14.0, TreeStar, San Carlos, CA, USA).
Cell population abundance	To ascertain cell population abundance, the sorted cells were directly observed under a fluorescent microscope.
Gating strategy	The small debris were removed by gating in the FSC/BSC axis, and the doublets were gated out using the axis of FSC-A/FSC-W and BSC-A/BSC-W. A positive region for each antibody staining was defined as a region that contained almost no cells (e.g., < 1.0%) stained with the corresponding isotype control antibody.

☒ Tick this box to confirm that a figure exemplifying the gating strategy is provided in the Supplementary Information.